Spin decoherence and off-resonance behavior of radio-frequency-driven spin rotations in storage rings

N. N. Nikolaev,[1] F. Rathmann,[2,*] J. Slim,[3,†] A. Andres,[2,3] V. Hejny,[2] A. Nass,[2] A. Kacharava,[2] P. Lenisa,[4] J. Pretz,[2,3] A. Saleev,[4,‡] V. Shmakova,[4,§] H. Soltner,[5] F. Abusaif,[2,3,‖] A. Aggarwal,[6] A. Aksentev,[7] B. Alberdi,[2,3,¶] L. Barion,[4] I. Bekman,[2,**] M. Beyß,[2,3] C. Böhme,[2] B. Breitkreutz,[2,‡] N. Canale,[4] G. Ciullo,[4] S. Dymov,[4] N.-O. Fröhlich,[2,†] R. Gebel,[2] M. Gaisser,[3] K. Grigoryev,[2,‡] D. Grzonka,[2] J. Hetzel,[2] O. Javakhishvili,[8] V. Kamerdzhiev,[2,‡] S. Karanth,[6] I. Keshelashvili,[2,‡] A. Kononov,[4] K. Laihem,[3,‡] A. Lehrach,[2,3] N. Lomidze,[9] B. Lorentz,[10] G. Macharashvili,[9] A. Magiera,[6] D. Mchedlishvili,[9] A. Melnikov,[7] F. Müller,[2,3] A. Pesce,[2] V. Poncza,[2] D. Prasuhn,[2] D. Shergelashvili,[9] N. Shurkhno,[2,‡] S. Siddique,[2,3,‡] A. Silenko,[11] S. Stassen,[2] E. J. Stephenson,[12] H. Ströher,[2] M. Tabidze,[9] G. Tagliente,[13] Y. Valdau,[2,‡] M. Vitz,[2,3] T. Wagner,[2,3,‡] A. Wirzba,[2,14] A. Wrońska,[6] P. Wüstner,[5] and M. Żurek[2,††]

(JEDI Collaboration)

[1]*L.D. Landau Institute for Theoretical Physics, 142432 Chernogolovka, Russia*
[2]*Institut für Kernphysik, Forschungszentrum Jülich, 52425 Jülich, Germany*
[3]*III. Physikalisches Institut B, RWTH Aachen University, 52056 Aachen, Germany*
[4]*University of Ferrara and Istituto Nazionale di Fisica Nucleare, 44100 Ferrara, Italy*
[5]*Zentralinstitut für Engineering, Elektronik und Analytik, Forschungszentrum Jülich, 52425 Jülich, Germany*
[6]*Marian Smoluchowski Institute of Physics, Jagiellonian University, 30348 Cracow, Poland*
[7]*Institute for Nuclear Research, Russian Academy of Sciences, 117312 Moscow, Russia*
[8]*Department of Electrical and Computer Engineering, Agricultural University of Georgia, 0159 Tbilisi, Georgia*
[9]*High Energy Physics Institute, Tbilisi State University, 0186 Tbilisi, Georgia*
[10]*GSI Helmholtzzentrum für Schwerionenforschung, 64291 Darmstadt, Germany*
[11]*Bogoliubov Laboratory of Theoretical Physics, Joint Institute for Nuclear Research, 141980 Dubna, Russia*
[12]*Indiana University, Department of Physics, Bloomington, Indiana 47405, USA*
[13]*Istituto Nazionale di Fisica Nucleare sez. Bari, 70125 Bari, Italy*
[14]*Institute for Advanced Simulation, Forschungszentrum Jülich, 52425 Jülich, Germany*

(Received 17 October 2023; accepted 18 October 2024; published 19 November 2024)

High-frequency driven resonant spin rotators are routinely used as standard instruments in polarization experiments in particle and nuclear physics. Maintaining the continuous exact parametric spin resonance condition of the equality of the spin rotator and the spin precession frequency during operation is one of the challenges. We present a detailed analytical description of the effects of detuning the exact spin resonance on the precessing vertical and in-plane components of the polarization. An important part of the formalism presented here is the consideration of experimentally relevant spin decoherence effects. Within the developed formalism, we address the impact of feedback via pilot-bunch-based comagnetometry on

[*]Contact author: frathmann@bnl.gov
Present address: Brookhaven National Laboratory, Upton, NY 11973, USA.
[†]Present address: Deutsches Elektronen-Synchrotron, 22607 Hamburg, Germany.
[‡]Present address: GSI Helmholtz Centre for Heavy Ion Research, 64291 Darmstadt, Germany.
[§]Present address: Brookhaven National Laboratory, Upton, NY 11973, USA.
[‖]Present address: Karlsruhe Institute of Technology, 76344 Eggenstein-Leopoldshafen, Germany.
[¶]Present address: Humboldt-Universität zu Berlin, Institut für Physik, 12489 Berlin, Germany.
[**]Present address: Zentralinstitut für Engineering, Elektronik und Analytik, Forschungszentrum Jülich, Jülich, Germany.
[††]Present address: Lawrence Berkeley National Laboratory, Berkeley, California 94720, USA.

continuous spin flips and on the related interpretation of charged-particle electric dipole moment searches using storage rings. We propose a spin-flip-based tomography of the longitudinal profile of polarization in a bunch, which is important for the evaluation of the polarization-dependent luminosity in collider experiments. We emphasize the potential importance of the previously unexplored phase of the horizontal polarization of the envelope as an indicator of the stability of radio-frequency-driven spin rotations in storage rings and as a testing ground for spin decoherence mechanisms.

DOI: 10.1103/PhysRevAccelBeams.27.111002

I. INTRODUCTION

Controlled spin rotations, notably the spin flips (SF), are imperative for particle and nuclear physics experiments that involve polarized particles (see, e.g., [1], for extensive reviews, see [2,3]). In storage rings, the rf magnetic field resonant to the idle spin precession acts as a spin flipper, resembling the familiar case of nuclear magnetic resonance (NMR) [4–7]. In an ideal magnetic ring, one stores beam particles with on average vertically oriented polarization, and the spin precession frequency is given by $f_s = G\gamma f_{rev}$, where f_{rev} denotes the revolution frequency of the ring, and G and γ denote magnetic anomaly and relativistic γ-factor of the stored particles [8].

In practice, the magnetic field imperfections in the machine, especially the ones tangential to the beam orbit, bring about a substantial and often poorly known correction to the above simple formula for f_s [2,3,9]. There are other complications that contribute, such as spin decoherence due to beam momentum spread $\Delta p/p$ from synchrotron oscillations and from orbit lengthening due to betatron oscillations, which require chromaticity tuning [10–12]. A more fundamental obstacle is that the beam energy is so poorly known that, rather conversely, the spin precession frequency can be used to calibrate the beam energy [13]. For instance, this problem of f_s being uncertain can be overcome with the Froissart-Stora scan approach, where the particle spin is subjected to a magnetic field of slowly varying frequency [14]. When the scanned frequency range is sufficiently broad to cover the not so well-known spin precession frequency f_s, then during the scan, the nuclear magnetic resonance condition will be encountered.

There are important spin-physics experiments in storage rings being conducted or anticipated, where it is imperative to maintain the exact spin-resonance condition for a long time, including a large number of SFs under continuous operation of an rf spin rotator. The present study was largely motivated by the program of the JEDI collaboration [15] to investigate systematic effects in the search for the electric dipole moment (EDM) of charged particles in storage rings, which is carried out at the cooler synchrotron (COSY) storage ring at Forschungszentrum Jülich [16,17] (see Fig. 1). As a part of this program, the JEDI collaboration has developed a technique to measure the idle spin-precession frequency with an accuracy of 10^{-10} within a

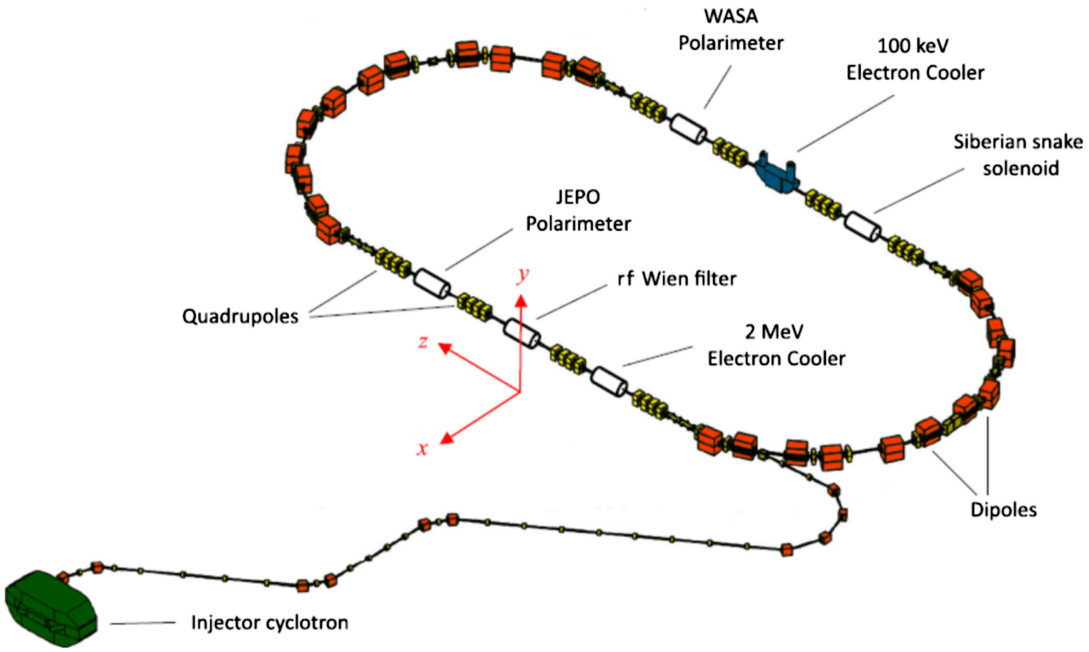

FIG. 1. Schematic diagram of the cooler synchrotron COSY as an example of a storage ring with rf Wien filter as a spin flipper and internal polarimeter. (Figure taken from Ref. [21] and slightly modified.).

time interval of 100 s [18,19]. When interacting with an internal polarimeter target, the precessing *horizontal* polarization component of the beam leads to an up-down asymmetry in the polarimeter detector system that oscillates with the spin-precession frequency (see Refs. [18–20] for details). A Fourier analysis of the time-stamped events in the polarimeter allows the determination of the oscillation frequency and also the envelope of the precessing polarization.

The knowledge of the spin-precession frequency makes it possible to excite spin flips with rf spin rotators. The EDM signal is the rotation of the spin in an electric field, and even in a purely magnetic storage ring, such as COSY, the spin-flip frequency is sensitive to the EDM of the stored particles [22,23] (for a review article, see [24]). However, if the spins are closely aligned along the *vertical* axis in the machine during a single or multiple spin flips [25], the control of the spin-precession frequency fails because in this case the horizontal polarization component is either too small or disappears completely. To go beyond the first quarter of the spin-flip period, comagnetometry must be invoked. A closely related problem is the feedback required to compensate for the phase shift of the spin-precession frequency caused by instabilities of the ring [18,19], which is also relevant for special so-called EDM rings with frozen spin [24,26–28].

Recently, the JEDI collaboration has proposed a solution to the problem of comagnetometry based on the so-called pilot bunch approach, which is applicable to a situation with multiple bunches stored in the ring [29]. The spin manipulations applied to the orbiting particles can be organized in three stages: (i) In the first stage, the initial vertical spins of multiple bunches of the stored deuterons are rotated into the horizontal plane by an rf solenoid, operated as a fixed-frequency spin rotator, like in the previous JEDI experiments. (ii) In the second stage, the frequency f_s of the spin idle precession of the (horizontal) in-plane polarization is measured. (iii) In the third stage, the rf Wien filter (WF) is used as a Lorentz-force free, and thus orbit preserving, spin rotator [30–32] in a special mode where it is switched off once per beam revolution for a short period of time when one of several stored bunches (pilot bunch) passes through the spin rotator. The operation of the WF starts at the frequency $f_{WF} = f_s$ as measured in stage II and is kept locked to the continuously measured spin-precession frequency f_s of the *unperturbed* (pilot) bunch. The pilot bunch, therefore, acts as a co-magnetometer, providing information about f_s that can be used as an input signal for a feedback system that ensures that the signal bunches are exposed to WF rf fields, which operates at frequency $f_s = f_{WF}$.

The pilot-bunch technique was proposed primarily in connection to the precision spin experiments on tests of fundamental symmetries, such as a search for the parity and time-reversal-invariance violating permanent EDMs of charged particles [24,26–28,33], but it may find other applications in spin physics at storage rings.

In practice, a certain amount of detuning is an indispensable feature of the rf-driven spin dynamics in storage rings. The frequency of rf power supplies can only be controlled with finite accuracy, leaving room for residual detuning of the WF and spin precession frequencies. Moreover, the betatron and synchrotron oscillation-induced spin tune spread is endemic in ensembles of stored particles. Finally, the process of feedback to lock the WF and spin precession phases is nothing more than a continuous compensation of the detuning caused by the instabilities of the storage ring. It is important to assess the impact of constant or time-varying detuning of individual particles in the ensemble on various aspects of the long-time continuous spin flips, ranging from the amplitude and tunes of the vertical spin oscillations to the time dependence of the envelope and phase of the precessing horizontal polarization. A very different effect of synchrotron oscillations, namely their impact on single Froissart-Stora crossings of the spin resonance [14] and the behavior of the polarization in the relatively short time periods thereafter, was studied earlier at COSY [34].

Yet, another closely related issue is the role of the finite spin-coherence time. For instance, damping is known to shift the frequency of the classical harmonic oscillator. In the case of a parametric spin resonance, involving non-commuting spin rotations, this requires a dedicated treatment of the impact of spin decoherence on the spin precessions and its dependence on the mechanism leading to spin decoherence.

Considering the JEDI experiments with polarized deuterons at a beam momentum of $p = 0.97$ GeV/c, the hierarchy of typical frequencies involved is listed in Table I. The typical time scales involved are the spin observation times (cycle times) $t_{exp} \approx 100$ s and the in-plane (horizontal) spin-coherence time $\tau_{SCT} \sim 1000$ s.

The experimental investigations revealed a non-negligible variation of the idle spin precession frequency of the order of about 10^{-8} from one fill to another and during each fill [18]. The feedback (fb) to synchronize the rf WF with the spin precession frequency introduces another frequency

TABLE I. Hierarchy of typical frequencies.

System	Frequency	Value (Hz)
Beam revolution	f_{rev}	750 000
Spin precession with respect to particle momentum	f_s	120 000
Synchrotron motion	f_{sy}	200
Feedback frequency	f_{fb}	0.2
rf-driven spin flip	f_{SF}	0.1
Feedback system induced spin precession spread	Δf_s^{fb}	0.010

scale $f_{\rm fb}$. Several consecutive measurements within a time interval of $t_{\rm fb} \sim 3$ s with a spin phase spread of the order of $\sigma_{\rm fb} \sim 0.2$ rad are necessary to correct the WF frequency during the next time interval $t_{\rm fb}$ [20]. The full feedback period of $2t_{\rm fb}$ defines the feedback frequency

$$f_{\rm fb} = \frac{1}{2t_{\rm fb}} \sim 0.2 \ \text{Hz}, \tag{1}$$

and the corresponding spread of the spin-precession frequency, which is of the order of

$$\Delta f_{\rm s}^{\rm fb} \sim \frac{\sigma_{\rm fb}}{2\pi t_{\rm fb}} \sim 10 \ \text{mHz}. \tag{2}$$

A similar hierarchy was observed for polarized protons at a beam kinetic energy of 49.3 MeV in COSY, where 99 successive flips driven by an rf solenoid were performed within 300 s. Assuming exponential attenuation of polarization, the average spin flipper efficiency was found to be $\epsilon_{\rm flip} = 0.9872 \pm 0.0001$ [17], corresponding to a lifetime of the continuously flipping spin of $\tau_{\rm flip} \approx 240$ s. With the rf spin flipper turned off, the vertical polarization was found to have a much longer lifetime of $\tau_{\rm p} = (2.7 \pm 0.8) \times 10^5$ s, Eq. (40) in [17]. Such a change of polarization lifetime by about three orders in magnitude is a clear indication of a close link between depolarization and spin-flip dynamics.

The hierarchy of frequencies given above (Table I) allows one to pursue all aspects of the rf-driven spin dynamics within a unified Bogoliubov-Krylov (BK) averaging approach [35] and paves the way to the first fully analytic and compact formalism for the detuned rf-driven parametric spin resonance taking into account

TABLE II. Glossary of frequently used parameters and variables. Typical numerical values of frequencies are given in Table I and derived auxiliary variables are omitted.

Parameter/variable	Notation	Defined in or near
Spin precession feedback period	$t_{\rm fb}$	Eq. (1)
Spin precession phase walk during feedback period	$\sigma_{\rm fb}$	Eq. (1)
Turn number	n	Eq. (3)
Spin tune	$\nu_{\rm s}$	Eq. (3)
Spin phase increment per turn	$\theta_{\rm s}$	Eq. (3)
Spin stable axis	$\vec{e}_{\rm s}$	Eq. (3)
Axis of spin rotation in WF	$\vec{w}$	Eq. (6)
WF phase increment per turn	$\theta_{\rm WF}$	Eq. (6)
WF tune	$\nu_{\rm WF}$	Eq. (7)
WF side band	K	Eq. (7)
Spin kick in the WF	$\chi_{\rm WF}$	Eq. (7)
Gyromagnetic anomaly of a particle $G = (g-2)/2$	G	Introduction, Eq. (7)
Beam velocity in units of the speed of light	β	Eq. (7)
Relativistic factor	γ	Eq. (7)
Polarization vector	$\vec{S}$	Eqs. (3) and (9)
Polarization envelope	$\vec{p}$	Eq. (9)
Spin-flip oscillation phase	x	Eqs. (18) and (30)
Spin-flip tune on the exact spin resonance	$\nu_{\rm SF}^0$	Eq. (19)
Initial phase of the in-plane polarization	$\Phi_{\rm in}$	Eq. (21)
Spin precession vs WF frequency detuning parameter	δ	Eq. (25)
Spin-flip tune off the exact spin resonance	$\nu_{\rm SF}$	Eq. (31)
Angle of orientation of the spin envelope precession axis	ρ	Eqs. (29) and (32)
Shift of the spin-flip symmetric interval $x \in [\zeta, 2\pi + \zeta]$	ζ	Eq. (41)
In-plane polarization envelope phase during continuous spin flips	$\phi(x)$	Eq. (45)
In-plane polarization damping per turn in the Bloch approximation	Γ	Eqs. (81) and (82)
Spin coherence time	$\tau_{\rm SCT}$	Eqs. (82) and (124)
Fractional revolution phase of a particle	ϕ	Eq. (92)
Slip factor	η	Eq. (99)
Gaussian rms width of the synchrotron oscillation amplitude distribution	$\sigma_{\rm sy}$	Eq. (101)
Amplitude of the synchrotron oscillations in the spin precession phase	$\psi_{\rm sy}$	Eq. (102)
Normalized synchrotron oscillation amplitude	ξ	Eq. (102)
Synchrotron oscillation amplitude distribution function	$F(\xi)$	Eq. (103)
Parameter of the synchrotron oscillation driven slip of the WF phase	$C_{\rm WF}$	Eq. (104)
Synchrotron oscillation strength in the spread of the spin-flip phase	$Q_{\rm sy}$	Eqs. (115) and (116)
Tilt of the spin stable axis by the electric dipole moment of a particle	$\xi^{\rm EDM}$	Eq. (144)

the decoherence of the polarization, thus extending the extending earlier considerations considerably [9,25,36,37]. There is a strong need for such a description because fitting the experimental data with multiple spin flips requires large number of calls of the spin evolution code, which cannot be readily met by the numerical solution of the spin evolution for up to $\sim 10^8$ revolutions of the beam. To this end, we emphasize that the above specified conditions are about typical for storage rings dedicated to the search for the charged particles electric dipole moments [24,26,27]. We regard our formalism as a toolbox for the determination of the detuning parameter for individual fills of a machine, and it may find applications in accelerator physics beyond the description of the pilot bunch regime.

Synchrotron oscillations (SO) entail an SO amplitude-dependent depolarization of particles in the bunch, and it was pointed out earlier how partial depolarization of the pilot bunch in the regime of incomplete masking (gating-out) of the rf of the spin rotator will open a way toward a tomography of the longitudinal profile of the bunch polarization. Evidently, a nonuniform longitudinal bunch polarization profile colliding bunches will affect the calibration of double polarization observables, for instance, in polarized deep inelastic scattering at the EIC. Such a tomography has not been discussed before, and it will be complementary to the corresponding transverse polarization profile of the bunch observed at RHIC [38], discussed in Ref. [39]. We pay particular attention to the as yet unexplored role of the phase of the spin envelope of the horizontal polarization on the control of the stable performance of rf-driven spin rotations, for which we provide a fully analytic description. This phase motion is expected to exhibit a strong sensitivity to detuning and to spin decoherence mechanisms.

A glossary of frequently used parameters and variables can be found in Table II, and the further presentation is structured as follows. In Sec. II, we present basics of the BK averaging approach to continuous spin flips in a form best suited for the interpretation of experimental data in the regime of detuned resonances. Section III contains an introduction to the main effects stemming from frequency detuning. Manifestations of detuning in the polarimetry of the in-plane polarization, most crucial for the pilot-bunch technique, are treated in Sec. IV. The impact of spin decoherence on spin flip is treated in Sec. V. The reduction of the spin-flip frequency by the feedback system to compensate for the walk of the spin-precession frequency that are caused by ring instabilities is discussed in Sec. VI. In Sec. VII, we discuss spin-flip tomography along the length of the bunch and depolarization of the pilot bunch caused by incomplete gating-out of the rf WF. The impact of the derived formalism on the interpretation of the precursor EDM experiments is explored in Sec. VIII. In Sec. IX, the main results are summarized.

II. STROBOSCOPIC SPIN EVOLUTION IN THE OFF-RESONANCE REGIME

A. Master equation

The average polarization $\vec{S}$ of an ensemble of particles in a storage ring points along the local stable spin axis $\vec{e}_s$. The one-turn evolution of the spin $\vec{S}$ consists of the idle precession by an angle $\theta_s = 2\pi\nu_s$ about the spin stable axis $\vec{e}_s$, followed by the stroboscopic spin kick in the orbit-preserving rf WF, which is used as a spin flipper and is located in a straight section of the ring. Here $\nu_s = f_s/f_{rev}$ denotes the spin tune, i.e., the number of spin precessions with respect to particle momentum per revolution. The length of the WF is negligibly small compared to the ring circumference and it acts on the spin stroboscopically once per turn. As an introduction to the subject, in this section, we describe the rf excited spin rotations in the SO(3) formalism [37] (for the alternative spinor formalism see [40], textbook [2], and Ref. [9]).

The stroboscopic master equation for the spin vector $\vec{S}(n)$ as a function of the turn number n is given by

$$\vec{S}(n) = \mathbf{R}_{\mathrm{WF}}(n)\mathbf{R}_s(\theta_s)\vec{S}(n-1), \tag{3}$$

where $\mathbf{R}_s(\theta_s)$ and $\mathbf{R}_{\mathrm{WF}}(n)$ are the ring and WF spin transfer matrices, respectively. Alongside $\vec{e}_s$, we define the radial unit vector $\vec{e}_r$ and the longitudinal unit vector $\vec{e}_t$ (tangential to the orbit), $\vec{e}_t = \vec{e}_r \times \vec{e}_s, \vec{e}_r = \vec{e}_s \times \vec{e}_t$. The vectors $\vec{e}_r$ and $\vec{e}_t$ define the spin precession plane. Because of the magnetic field imperfections in the ring lattice, the orientation of $\vec{e}_s$ differs slightly from $\vec{e}_y$, the normal one to the storage ring plane, also known as the $\{\vec{e}_x, \vec{e}_z\}$ momentum plane, see Fig. 1, and the spin precession plane is tilted with respect to the ring plane [37]. Wherever relevant, we will distinguish between the spin and momentum bases, and our reference to $\vec{e}_s$ as the *vertical* direction, and to the components of the spin in the spin precession plane as the *horizontal* (in-plane) ones, should not cause any confusion. We start with a particle on the reference orbit and in the approximation of vanishing spin decoherence. The idle precession spin transfer matrix per turn is given by

$$\mathbf{R}_s(\theta_s) = \begin{pmatrix} \cos\theta_s & 0 & \sin\theta_s \\ 0 & 1 & 0 \\ -\sin\theta_s & 0 & \cos\theta_s \end{pmatrix} \tag{4}$$

with two precessing in-plane polarization eigenvectors

$$\begin{aligned} \vec{u}_r(n) &= \vec{e}_r \cos(\theta_s n) + \vec{e}_t \sin(\theta_s n), \\ \vec{u}_t(n) &= -\vec{e}_r \sin(\theta_s n) + \vec{e}_t \cos(\theta_s n), \end{aligned} \tag{5}$$

where n is the turn number. The rf WF rotates spin about axis $\vec{w}$ is along its magnetic field $\vec{B}_{\mathrm{WF}}$ with the rotation angle (spin kick)

$$\chi(n) = \chi_{\rm WF}\cos(\theta_{\rm WF} n) \tag{6}$$

with the amplitude

$$\chi_{\rm WF} = -\frac{q(1+G)}{m\gamma^2\beta c}\int dl B_{\rm WF}, \tag{7}$$

where $B_{\rm WF}$ is the amplitude of magnetic field in the WF, c is the speed of light, q, m, β, and G are the charge, mass, velocity, and magnetic anomaly of the orbiting particles, respectively. The WF is operated at the frequency $f_{\rm WF}$, the WF tune is given by $\nu_{\rm WF} = f_{\rm WF}/f_{\rm rev}$ and $\theta_{\rm WF} = 2\pi\nu_{\rm WF}$. Evidently, the spin rotation in the WF is identical for all side bands $\nu_{\rm WF} \Rightarrow \nu_{\rm WF} + K, K = 0, \pm 1, \pm 2, \ldots$ Without loss of generality, we can focus the discussion on the so-called magnetic-dipole moment (MDM) mode, when $\vec{w} = \vec{e}_{\rm r}$ and $|\vec{e}_{\rm s} \times \vec{w}| = 1$. The corresponding spin transfer matrix for pass n through the WF equals

$$\mathbf{R}_{\rm WF}(n) = \begin{pmatrix} 1 & 0 & 0 \\ 0 & \cos\chi(n) & -\sin\chi(n) \\ 0 & \sin\chi(n) & \cos\chi(n) \end{pmatrix} = 1 + \mathbf{W}(n). \tag{8}$$

B. Bogoliubov-Krylov averaging for exact spin resonance

The above outlined hierarchy of spin evolution frequencies (Table I) dictates invoking the Bogoliubov-Krylov (BK) averaging [35] as a tool for a solution of the master equation (3). The starting point is the interaction representation

$$\vec{S}(n) = |\vec{S}(0)|\mathbf{R}_{\rm s}(n\theta_{\rm WF})\vec{p}(n), \tag{9}$$

where $\vec{p}(n)$ is the spin envelope with initial condition $|\vec{p}(0)| = 1$. The envelope $\vec{p}(n)$ is the polarization as seen by an observer in the co-rotating spin reference frame rotating about the axis $\vec{e}_{\rm s}$ with frequency $f_{\rm WF}$

$$\vec{S}(n) = |\vec{S}(0)|\{p_{\rm r}(n)\vec{u}_{\rm r}(n) + p_{\rm s}(n)\vec{e}_{\rm s} + p_{\rm t}(n)\vec{u}_{\rm t}(n)\}, \tag{10}$$

where $\vec{u}_{\rm r,t}(n)$ are counterparts of $\vec{e}_{\rm r,t}$ and are defined by Eq. (5) in terms of $\theta_{\rm WF}$ instead of $\theta_{\rm s}$. Without loss of generality, in the following, we set $|\vec{S}(0)| = 1$.

This particular choice of the co-rotating frame is dictated by the point that $f_{\rm WF}$ is the only *known* primary frequency in the problem. The spread of spin tunes in the bunch and the *unknown* walk of the spin precession frequency $f_{\rm s}$ necessitate a continuous (stroboscopic once per turn) measurement of this *unknown* $f_{\rm s}$ in order to obtain a feedback for setting the WF to another known frequency, etc. To the extent that intrabeam interactions are weak to depolarize the beam (see for instance Ref. [17] and the related discussion in Sec. I), the bunch can be treated as an ensemble of independent particles so that we solve first the one-particle problem and then take the average over the ensemble.

We illustrate the BK averaging on the case of exact resonance $\nu_{\rm s} = \nu_{\rm WF}$ following the treatment in Ref. [9]. Master equation for the spin envelope takes the form

$$\vec{p}(n) = \mathbf{R}_{\rm s}(-n\theta_{\rm WF})\mathbf{R}_{\rm WF}(n)\mathbf{R}_{\rm s}(n\theta_{\rm WF})\vec{p}(n-1). \tag{11}$$

In view of $\chi_{\rm WF} \ll 1$, the envelope evolution is slow and the stroboscopic Eq. (11) can be cast in the differential form

$$\frac{\vec{p}(n)}{{\rm d}n} = \mathbf{R}_{\rm s}(-n\theta_{\rm WF})\mathbf{W}(n)\mathbf{R}_{\rm s}(n\theta_{\rm WF})\vec{p}(n). \tag{12}$$

To the leading order in the small parameter $\chi_{\rm WF}$, the BK averaging over the spin precession periods proceeds as follows:

$$\begin{aligned}\langle \mathbf{R}_{\rm s}(-n\theta_{\rm WF}n)\mathbf{W}(n)\mathbf{R}_{\rm s}(n\theta_{\rm WF}n)\rangle &= \left\langle \begin{pmatrix} 0 & -\chi(n)\sin(n\theta_{\rm WF}) & 0 \\ \chi(n)\sin(n\theta_{\rm WF}) & 0 & -\chi(n)\cos(n\theta_{\rm WF}) \\ -0 & \chi(n)\cos(n\theta_{\rm WF}) & 0 \end{pmatrix} \right\rangle \\ &= \begin{pmatrix} 0 & 0 & 0 \\ 0 & 0 & -\frac{1}{2}\chi_{\rm WF} \\ -0 & \frac{1}{2}\chi_{\rm WF} & 0 \end{pmatrix} = 2\pi\nu_{\rm SF}\begin{pmatrix} 0 & 0 & 0 \\ 0 & 0 & -1 \\ 0 & 1 & 0 \end{pmatrix} = 2\pi\nu_{\rm SF}\mathbf{U}, \end{aligned} \tag{13}$$

where we applied

$$\langle\cos^2(\theta_{\rm WF}n)\rangle = \frac{1}{2} \quad \text{and} \quad \langle\cos(\theta_{\rm WF}n)\sin(\theta_{\rm WF}n)\rangle = 0. \tag{14}$$

The solution of Eq. (12) for the envelope will be

$$\vec{p}(x) = \exp(2\pi\nu_{\rm SF}n\mathbf{U})\vec{p}(0) = \mathbf{E}_0(x)\vec{p}(0), \tag{15}$$

where the subscript 0 stands for zero detuning. Making use of the recursive relations:

$$\mathbf{U}^{2n+1} = (-1)^n\mathbf{U}, \qquad \mathbf{U}^{2n} = (-1)^{n-1}\mathbf{U}^2, \tag{16}$$

we obtain

$$\mathbf{E}_0(x) = \begin{pmatrix} 1 & 0 & 0 \\ 0 & \cos x & -\sin x \\ 0 & \sin x & \cos x \end{pmatrix}, \tag{17}$$

and

$$x = 2\pi\nu^0_{\mathrm{SF}} n = 2\pi\nu^0_{\mathrm{SF}} f_{\mathrm{rev}} t \tag{18}$$

is the SF phase with the SF tune

$$\nu^0_{\mathrm{SF}} = \frac{1}{4\pi}\chi_{\mathrm{WF}}|\vec{e}_{\mathrm{s}} \times \vec{w}|, \tag{19}$$

which defines the SF frequency $f_{\mathrm{SF}} = \nu^0_{\mathrm{SF}} f_{\mathrm{rev}}$. The factor $|\vec{e}_{\mathrm{s}} \times \vec{w}|$ emerges for generic orientation of the WF axis $\vec{w}$ [9,37]. For instance, the so-called EDM mode corresponds to $\vec{w} \approx \vec{e}_{\mathrm{s}} \approx \vec{e}_{\mathrm{y}}$. The master equation (3) describes sequential rotations with preservation of the magnitude of the polarization, and the matrix (17) preserves this unitarity property.

Note that SFs proceed via rotation of the vertical envelope to the tangential one with the frequency f_{SF}, while the radial envelope remains a spectator:

$$\begin{aligned} p_{\mathrm{r}}(x) &= p_{\mathrm{r}}(0), \\ p_{\mathrm{s}}(x) &= p_{\mathrm{s}}(0)\cos x - p_{\mathrm{t}}(0)\sin x, \\ p_{\mathrm{t}}(x) &= p_{\mathrm{s}}(0)\sin x - p_{\mathrm{t}}(0)\cos x. \end{aligned} \tag{20}$$

It is convenient to define the initial spin precession phase Φ_{in} such that

$$\begin{aligned} p_{\mathrm{r}}(0) &= p_{\mathrm{rt}}(0)\cos\Phi_{\mathrm{in}}, \\ p_{\mathrm{t}}(0) &= p_{\mathrm{rt}}(0)\sin\Phi_{\mathrm{in}}. \end{aligned} \tag{21}$$

where $p_{\mathrm{rt}} = \sqrt{p_{\mathrm{r}}^2 + p_{\mathrm{t}}^2}$ denotes the modulus of the in-plane polarization. These features of the rf driven polarization are shown in Fig. 2. For pure in-plane initial polarization $p_{\mathrm{s}}(0) = 0$, the envelope of the vertical polarization evolves as $p_{\mathrm{s}}(x) = -\sin\Phi_{\mathrm{in}}\sin x$. The final polarization is given by

$$\vec{S}(n) = \mathbf{R}_{\mathrm{s}}(n\theta_{\mathrm{WF}})\mathbf{E}_0(x)\vec{S}(0), \tag{22}$$

and in the absence of spin decoherence mechanisms, $\vec{S}(n)$ can be regarded as an average polarization of an ensemble (bunch) of particles.

The BK averaging of the exact expression $\sin\chi(n)\cos(n\theta_{\mathrm{WF}})$, instead of the perturbative expression $\chi(n)\cos(n\theta_{\mathrm{WF}})$, gives

$$\langle \sin\chi(n)\cos(n\theta_{\mathrm{WF}})\rangle = J_1(\chi_{\mathrm{WF}}), \tag{23}$$

where $J_1(z)$ is the familiar Bessel function of the first kind. For conditions of the typical JEDI experiments with deuterons, we have an extremely small argument in the Bessel function:

$$\frac{\chi_{\mathrm{WF}}}{2} = 2\pi\nu^0_{\mathrm{SF}} = 2\pi\frac{f_{\mathrm{SF}}}{f_{\mathrm{rev}}} \approx 10^{-6} \tag{24}$$

and the correction to the linear approximation for the SF tune amounts to $\approx 10^{-12}$. This time-independent correction can safely be neglected, see the related discussion of Eq. (107) in Sec. V C 2.

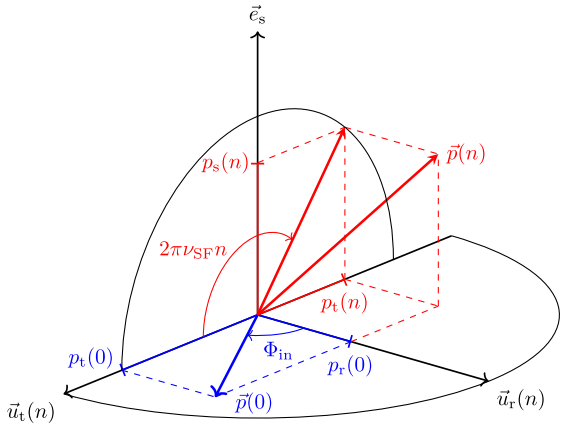

FIG. 2. Evolution of the spin envelope in the reference frame, co-rotating in the regime of exact spin resonance at the idle spin-precession frequency $f_{\mathrm{s}} = f_{\mathrm{WF}}$. The initial polarization $\vec{p}(0)$ is in the horizontal $\{\mathrm{rt}\}$ spin-precession plane. The spectator radial component $p_{\mathrm{r}}(0) = p(0)\cos\Phi_{\mathrm{in}}$ is immune to the rf WF and continues to precess unchanged. The active tangential component $p_{\mathrm{t}}(0) = p(0)\sin\Phi_{\mathrm{in}}$ starts rotations driven by the WF in the vertical $\{\mathrm{st}\}$ plane with the spin-flip frequency $f_{\mathrm{SF}} = \nu_{\mathrm{SF}} f_{\mathrm{rev}}$. To the observer in the co-rotating frame, the idly precessing unit vectors $\vec{u}_{\mathrm{r}}(n)$ and $\vec{u}_{\mathrm{t}}(n)$ appear as being constant along the radial and tangential directions.

C. Off-resonance spin rotations

Two *known* parameters of the SF dynamics are the WF frequency f_{WF} and the Wien-filter strength χ_{WF} (spin kick). We parameterize detuning of spin precession from WF by a small angle:

$$\delta = \theta_{\mathrm{s}} - \theta_{\mathrm{WF}} = 2\pi(\nu_{\mathrm{s}} - \nu_{\mathrm{WF}}) = 2\pi\frac{\Delta f_{\mathrm{s}}}{f_{\mathrm{rev}}}. \tag{25}$$

Correspondingly, we keep defining the interaction representation in terms of the *known* WF frequency as in Eq. (9) and cast the envelope evolution equation (11) in the form

$$\vec{p}(n) = \mathbf{R}_{\mathrm{s}}^{-1}(n\theta_{\mathrm{WF}})\mathbf{R}_{\mathrm{WF}}(n)\mathbf{R}_{\mathrm{s}}(\delta)\mathbf{R}_{\mathrm{s}}(n\theta_{\mathrm{WF}})\vec{p}(n-1). \tag{26}$$

Repeating the derivation of Eq. (17), we find

$$\mathbf{U} = \begin{pmatrix} 0 & 0 & \cos\rho \\ 0 & 0 & -\sin\rho \\ -\cos\rho & \sin\rho & 0 \end{pmatrix}, \tag{27}$$

which satisfies the recursive relations [Eq. (16)]. The above derived **U** satisfies the recursive relations from Eq. (16) so that application of the decomposition in Eq. (17) yields

$$\mathbf{E}(x)=\begin{pmatrix} E_{\rm rr}(x) & E_{\rm rs}(x) & E_{\rm rt}(x)\\ E_{\rm sr}(x) & E_{\rm ss}(x) & E_{\rm st}(x)\\ E_{\rm tr}(x) & E_{\rm ts}(x) & E_{\rm tt}(x)\end{pmatrix}=\begin{pmatrix} \sin^2\rho+\cos^2\rho\cos x & \cos\rho\sin\rho(1-\cos x) & \cos\rho\sin x\\ \cos\rho\sin\rho(1-\cos x) & \cos^2\rho+\sin^2\rho\cos x & -\sin\rho\sin x\\ -\cos\rho\sin x & \sin\rho\sin x & \cos x\end{pmatrix}, \tag{28}$$

which describes the envelope rotations about the axis (for generic SO(3) rotations, see Ref. [41])

$$\vec{m}=\sin\rho\vec{e}_{\rm r}-\cos\rho\vec{e}_{\rm s}, \tag{29}$$

with the SF phase

$$x=2\pi\nu_{\rm SF}n=2\pi\nu_{\rm SF}f_c t \tag{30}$$

(for generic SO(3) rotations, see Ref. [41]) and the SF flip tune

$$\nu_{\rm SF}=\frac{\sqrt{\chi_{\rm WF}^2+4\delta^2}}{4\pi}=\frac{\nu_{\rm SF}^0}{\sin\rho}. \tag{31}$$

The angle ρ is defined by

$$\sin\rho=\frac{\chi_{\rm WF}}{4\pi\nu_{\rm SF}},\qquad \cos\rho=\frac{2\delta}{4\pi\nu_{\rm SF}}. \tag{32}$$

We reiterate that in the generic case the substitution $\chi_{\rm WF}\Rightarrow|\vec{e}_{\rm s}\times\vec{w}|\chi_{\rm WF}$ is in order so that

$$\nu_{\rm SF}^2=\frac{1}{16\pi^2}(\chi_{\rm WF}^2|\vec{e}_{\rm s}\times\vec{w}|^2+4\delta^2). \tag{33}$$

In all cases, $t=0$ and $x=0$ correspond to the instant when the spin flipper is switched on.

An early derivation of Eq. (28) within the spinor formalism was published by JEDI in 2017 in Appendix A, Eq. (A20) of Ref. [9], and an alternative treatment of the same problem was reported in 2018 (Eqs. (4)–(7) in [25]). The SO(3) formalism outlined above, in conjunction with the BK technique, will play a central role in the subsequent inclusion of spin decoherence and feedback effects, which are discussed in Secs. V and VI.

D. Radiofrequency solenoid as a spin rotator

The above formalism is fully applicable as well to the orbit preserving rf solenoid as a spin rotator. In that case, one needs to interchange $\vec{e}_{\rm t}\Rightarrow\vec{e}_{\rm r}, \vec{e}_{\rm r}\Rightarrow-\vec{e}_{\rm t}$ and also the corresponding indices r $\Leftrightarrow$ t in the matrix elements of **E**. The spin kick $\chi_{\rm WF}$ in the WF must be swapped for the spin kick in the solenoid $\chi_{\rm sol}$

$$\chi_{\rm WF}\Rightarrow\chi_{\rm sol}=-\frac{q(1+G)}{mv}\int dzB(z), \tag{34}$$

where $B(z)$ is the longitudinal magnetic field in the solenoid. In the co-rotating frame of reference, the spin envelope would precess about the axis

$$\vec{m}=-\sin\rho\vec{e}_{\rm t}+\cos\rho\vec{e}_{\rm s}. \tag{35}$$

In the limit of vanishing detuning, $\cos\rho=0$, the spectator in-plane polarization will be directed along $\vec{e}_{\rm t}$. In addition, the convention for the initial spin phase has to be modified such that $\Phi_{\rm in}\rightarrow\Phi_{\rm in}+\pi/2$.

III. IMPACT OF DETUNING ON THE VERTICAL POLARIZATION

A. Evolution of vertical polarization

We start with the beam polarization stored along the spin stable axis $\vec{e}_{\rm s}$ so that $p_{\rm s}(0)=1$ and $p_r(0)=p_t(0)=0$. With continuously operating rf spin-flipper, either WF or solenoid, the vertical polarization will evolve as

$$p_{\rm s}(x)=E_{\rm ss}(x)p_{\rm s}(0)=(\cos^2\rho+\sin^2\rho\cos x)p_{\rm s}(0). \tag{36}$$

This result nicely illustrates the interplay of the detuning by δ [see Eqs. (25) and (32)] and the spin kick $\chi_{\rm WF}$ in the WF: (i) The envelope exhibits oscillations with amplitude $\sin^2\rho\leq 1$ on top of the offset $\cos^2\rho$. (ii) At large detuning, $\cos^2\rho>$ ½, the SF is incomplete: the offset term takes over and the vertical polarization no longer passes through zero. (iii) At small detuning, $\cos^2\rho<$ ½, the pure horizontal polarization is reached at the envelope phase

$$\cos x_0=-\cot^2\rho. \tag{37}$$

(iv) Conversely, to achieve the often-required $\pi/2$ rotation from the vertical to the horizontal spin orientation, usually performed on a time scale of approximately 1 s with the rf solenoid [42], the detuning needs to satisfy only the very liberal condition that

$$\Delta f_{\rm s}<\frac{1}{\sqrt{2}}f_{\rm SF}. \tag{38}$$

(v) The detuning can be determined by a comparison of the flipped, $S_{\rm s}(\pi)$, and initial, $S_{\rm s}(0)$, vertical polarizations:

$$2\cos^2\rho = 1 - \frac{S_s(\pi)}{S_s(0)}. \tag{39}$$

One caveat to such a comparison of two polarizations is that the measured vertical polarizations may have an offset caused by the instrumental asymmetries in the polarimeter.

B. Build-up of vertical polarization from in-plane polarization

In this case, the starting point is $p_{rt}(0) = 1$ and

$$\begin{aligned} p_s(x) &= E_{sr}(x)p_r(0) + E_{st}(x)p_t(0) \\ &= q(\Phi_{in},\rho)\sin\rho\sin\left(\frac{x}{2}\right)\sin\left(\frac{x}{2}-\zeta\right), \end{aligned} \tag{40}$$

where

$$\begin{aligned} q(\Phi_{in},\rho) &= \sqrt{\sin^2\Phi_{in} + \cos^2\rho\cos^2\Phi_{in}}, \\ \sin\zeta &= \frac{\sin\Phi_{in}}{q(\Phi_{in},\rho)}, \qquad \cos\zeta = \frac{\cos\rho\cos\Phi_{in}}{q(\Phi_{in},\rho)}. \end{aligned} \tag{41}$$

In the case of $\zeta = 0$, the vertical polarization is invariant under the interchange $x \Leftrightarrow 2\pi - x$ within the symmetric period interval $[0, 2\pi]$, while for finite ζ the related invariance under $x - \zeta \Leftrightarrow 2\pi - (x - \zeta)$ persists in the shifted symmetric interval $[\zeta, 2\pi + \zeta]$.

In the exceptional case of exact resonance, $\cos\rho = 0$:

$$p_s(x) = -p_t(0)\sin x = -\sin\Phi_{in}\sin x, \tag{42}$$

and only the initial tangential in-plane polarization is the active one, while the spectator radial component does not contribute at all to the build-up of the vertical polarization.

IV. POLARIMETRY OF THE IN-PLANE POLARIZATION

A. Amplitude and phase conventions

In the generic case, the polarization components are given by Eq. (22). Because of parity conservation in strong interactions, the tangential (longitudinal) polarization at the polarimeter $S_t(x,n)$ is not measurable. The up-down asymmetry in the polarimeter measures the radial (transverse) polarization component $S_r(x)$. This measurement takes place stroboscopically once per revolution of the beam. The polarimeter signal as a function of turn number n is Fourier-analyzed bin by bin, with a bin duration corresponding to about 10^6 turns in the machine, but still sufficiently short so that the variation of the spin-flip phase x and the walk of the in-plane-polarization envelopes $p_r(x)$ and $p_t(x)$ can be neglected.

A cartoon of the Fourier analysis boils down to the evaluation of

$$\begin{aligned} p_r(x) &= \frac{2}{N}\sum_{k=1}^{N} S_r(x,k)\cos k\xi_{WF}, \\ p_t(x) &= \frac{2}{N}\sum_{k=1}^{N} S_r(x,k)\sin k\xi_{WF}. \end{aligned} \tag{43}$$

where k is the turn number of the corresponding event in the polarimeter, and N is a total number of events in the bin [18–20]. These definitions are supported by the least squares analysis, and both $p_r(x)$ and $p_t(x)$ take their maximal magnitudes at $\xi_{WF} = \pm\theta_{WF}$. Because only one component of the rotating spin vector $\vec{S}(x,k)$ is observed, there is a nonessential sign ambiguity in $p_t(x)$.

The orientation of $\vec{p}_{rt}$ is given by the phase $0 < \psi(x) < 2\pi$, specified in terms of

$$\sin\psi(x) = \frac{p_r(x)}{p_{rt}(x)}, \qquad \cos\psi(x) = \frac{p_t(x)}{p_{rt}(x)}. \tag{44}$$

The full-fledged four-quadrant determination of $\psi(x)$ is well possible, but without any loss of information, it is convenient to map the phase $\psi(x)$ onto the band $0 < \phi(x) < \pi$, where

$$\phi(x) = \arccos[\cos\psi(x)]. \tag{45}$$

In terms of the four-quadrant definition, this amounts to assigning to the radial polarization its modulus:

$$|p_r(x)| = p_{rt}(x)|\sin\psi(x)| = p_{rt}(x)\sin\phi(x). \tag{46}$$

With limited statistics, the magnitude $p_{rt}(x)$ of the in-plane component of the close-to-vertical polarization can only be measured to a certain accuracy Δp_{rt}, and the accuracy of determination of the phase of $p_{rt}(x)$ deteriorates for small in-plane polarization, $\Delta\phi(x) \propto \Delta p_{rt}/p_{rt}$.

We focus here on the analytical treatment of the spin-decoherence-free case, however, Eqs. (44) and (45) for the envelope phase in terms of $p_{r,t}$ of Eq. (43) are fully applicable to scenarios involving spin decoherence, which are discussed in Sec. V. The related early considerations on phase motion in the spin-decoherence-free case with a comparison to experimental data were reported in the JEDI publication [25].

B. Continuous spin rotation by the WF: Build-up of pure initial in-plane polarization

It is instructive to look at the *continuous* spin rotations generated by the rf WF starting with the initial vertical polarization, $p_s(0) = 1$, and $p_r(0) = p_t(0) = 0$. In terms of the generic three-stage process, outlined in Sec. I, in stage I, the spins are rotated by into the horizontal plane, stage II is skipped altogether, and stage III begins at the instant of vanishing vertical polarization reached in stage I.

The detuning angle ρ is kept constant from stage I to stage III on.

The envelope rotation phase $x = 0$ corresponds to the time at which the spin rotator is switched on. The radial and tangential polarization envelopes are given by

$$p_r(x) = E_{rs}(x)p_s(0) = \cos\rho \sin\rho(1 - \cos x),$$
$$p_t(x) = E_{ts}(x)p_s(0) = \sin\rho \sin x p_s(0), \quad (47)$$

and

$$p_{rt}(x) = 2|\sin\rho|\cdot\left|\sin\frac{x}{2}\right|\sqrt{\cos^2\frac{x}{2} + \cos^2\rho\sin^2\frac{x}{2}}. \quad (48)$$

Although $p_r(x)$ is zero at $\cos x = 1$, in this regime, it does not change its sign at any value of x.

C. Interplay of vertical, tangential, and radial polarizations

The mathematically exact resonance condition, $\cos\rho = 0$, is an exceptional but still instructive case. In this case, the envelope rotation axis $\vec{m}$ of Eq. (29) is a purely radial one. Viewed in the co-rotating frame, the vertical polarization cannot rotate into the radial direction along the rotation axis [see Eq. (47)]. In other words, the spectator radial polarization decouples from the vertical polarization, while the active tangential envelope will oscillate with the full amplitude $p_s(0)$. Similarly, the tangential polarization cannot rotate into the radial one. However, this decoupling of both the vertical and the active in-plane spin components from the spectator in-plane is lifted as soon as $\cos\rho \neq 0$. In the former case, this is clear from Eq. (47). In the latter case, the cross talk of radial and tangential polarizations is given by the matrix elements $E_{rt}(x) = -E_{tr}(x)$ in Eq. (28). For instance, if $p_s(0) = p_r(0) = 0$ and $p_t(0) = 1$, then

$$p_r(x) = \cos\rho \sin\, x\, p_t(0). \quad (49)$$

Vice versa, at $p_s(0) = p_t(0) = 0$ and $p_r(0) = 1$, we find

$$p_t(x) = -\cos\rho \sin x p_r(0). \quad (50)$$

This cross talk derives from the vertical component $\cos\rho\vec{e}_s$ of the rotation axis $\vec{m}$ of the envelope.

D. Continuous spin rotation by the WF and envelope of in-plane polarization

The result for $p_{rt}(x)$ has already been given in Eq. (48). The predicted dependence of the spin envelope on the detuning is depicted in Fig. 3 for $\cos\rho \geq 0$. As a function of the phase x, the envelope $p_{rt}(x)$ is a periodic function with a period of 2π, but in order to better demonstrate the periodicity properties of the in-plane polarization, we show the results for $x \in [0, 4\pi]$.

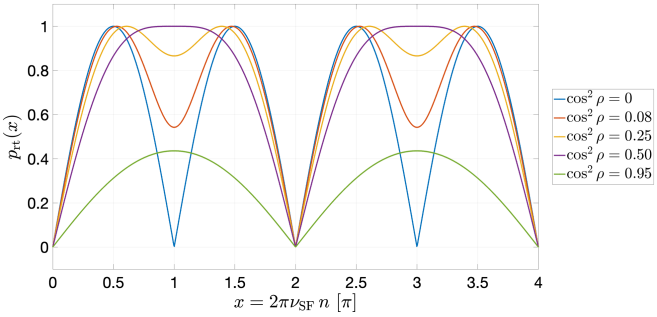

FIG. 3. Pattern of the time dependence of the envelope of the horizontal polarization, which evolves from the pure vertical initial polarization $p_s(0) = 1$, under the rf-driven continuous full or partial spin flips for different detuning, as given by Eq. (48). Note that the central zero of $p_{rt}(x)$ at $x = \pi$ and $x = 3\pi$ (full spin flip) occurs exclusively at zero detuning, i.e., for $\delta = 0$ or $\cos^2\rho = 0$. Within each period, the double hump structure with hump height $p_{rt} = 1$ persists for $\cos^2\rho < ½$. At even greater detuning, for $\cos^2\rho \geq ½$, $p_{rt}(x)$ exhibits a single hump whose height vanishes in the limit $\rho \to 0$.

For vanishing detuning, $\cos\rho = 0$, we recover the second line of Eq. (47):

$$p_{rt}(x) = 2\left|p_s(0)\sin\left(\frac{x}{2}\right)\cos\left(\frac{x}{2}\right)\right|. \quad (51)$$

In the interval $[0, 2\pi]$, the envelope has two end-point zeros at $x_1 = 0$ and $x_2 = 2\pi$, stemming from $\sin(x/2) = 0$. There is still another zero crossing at midpoint $x_3 = \pi$, stemming from $\cos(x/2) = 0$, which turns into minimum as soon as $\cos\rho \neq 0$. For $\sin^2\rho > 1/2$, a prominent double-hump structure with $p_{rt}(x_{4,5}) = 1$ at

$$x_{4,5}(\rho) = \pi \pm 2\arcsin\sqrt{1 - \frac{1}{2\sin^2\rho}} \quad (52)$$

remains in place until $\sin^2\rho = 1/2$, when the two humps merge into one. From this point on the vertical spin flip becomes incomplete, see (ii) in Sec. III A, and height of the single bump $p_{rt}(x) = |p_s(0)\sin 2\rho| < 1$.

E. Continuous spin rotation by the WF and phase of in-plane polarization

The expected phase motion for $\cos\rho > 0$ is depicted in Fig. 4 for several values of ρ. According to Eq. (47), in the considered case, the radial envelope does not change its sign at all, i.e., $\mathrm{sgn}(p_r(x)) = +1$, while $p_t(x)$ changes the sign at $x = \pi$. Still, at $x \neq \pi$, the phase remains well defined. Making use of $p_t(x)$ from Eq. (47) and $p_{rt}(x)$ from Eq. (48), we obtain

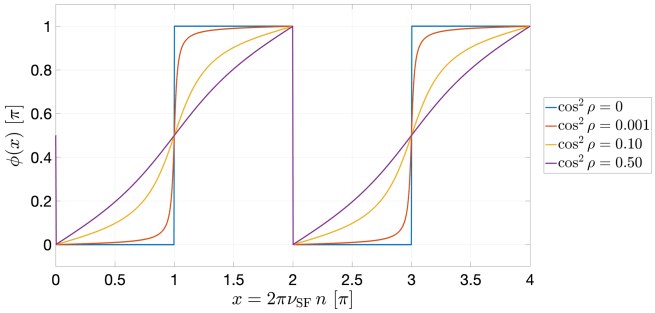

FIG. 4. Phase motion of the horizontal polarization envelope during the rf-driven continuous spin flips for different detuning, as predicted by Eq. (53) for $\cos\rho \in [0, 1]$. The phase exhibits a jump by $-\pi$ from $x = 2\pi - 0$ to $2\pi + 0$, which repeats itself periodically at any $x = 2\pi M$, where $M = 0, 1, 2, , 3, \ldots$ In the vicinity of the phase jump, the slope $\phi'(2\pi - 0) = \phi'(2\pi + 0) = \frac{1}{2}\cos\rho$. Yet another jump by $+\pi$ develops at $x = \pi + 2\pi M$, where the slope, $\phi'(x = \pi) = 2/\cos\rho$, of the phase becomes singular for $\cos^2\rho \to 0$.

$$\phi(x) = \arccos\left(\frac{\mathrm{sgn}(\sin x)\mathrm{sgn}(\sin\rho)}{\sqrt{1 + \cos^2\rho\tan^2\frac{x}{2}}}\right). \tag{53}$$

Evidently, the change of the sign, $\sin\rho \Leftrightarrow -\sin\rho$, entails the change of phase $\phi(x) \Leftrightarrow \pi - \phi(x)$. We predict $\cos\phi(x) = 0$ and $\phi(x) = \pi/2$ at $x \to \pi$, *regardless* of the detuning angle ρ. One readily finds that at $x = \pi$, the derivative of the phase equals $\phi'(x) = 2/\cos\rho$, which is singular at $\cos\rho \to 0$, thus the phase motion degenerates into the step function. Still more singular is the case of $x = 2\pi$, when

$$\cos\phi(x) = \mathrm{sgn}(\sin x)\mathrm{sgn}(\sin\rho) \tag{54}$$

and changes sign from -1 for $x = 2\pi - 0$ to $+1$ for $x = 2\pi + 0$, i.e., the envelope phase has a phase jump by $-\pi$ irrespective of the detuning. Finally, Eq. (53) predicts the slope at $x = +0$ and $x = 2\pi - 0$:

$$\phi'(+0) = \phi'(2\pi - 0) = \phi'(2\pi + 0) = \frac{1}{2}|\cos\rho|. \tag{55}$$

F. Interplay of detuning and initial phase in the generic three-stage regime

In NMR-like storage ring experiments on the search for charged particle, electric dipole moments (see Refs. [24,26,27] and Sec. VIII) and axionlike particles [43] of major interest are continuous spin flips or buildup of partial vertical polarization during stage III, where we make use of the rf WF starting with in-plane polarization, i.e., $p_s = 0$. Polarimetry of the idle spin precession during stage II gives access to the spin precession frequency and the orientation of the in-plane polarization at the activation of the WF in stage III. The JEDI collaboration developed a feedback to preserve the corresponding phase Φ_{in} to an accuracy of 0.21 rad [20]. The generic solution for the vertical polarization as a function of Φ_{in} is given by Eq. (40).

In the evolution of the horizontal polarization, the dependence on Φ_{in} is much more subtle and deserves a dedicated analysis.

1. Envelope of in-plane polarization

By recourse to the envelope evolution matrix $\mathbf{E}(x)$ of Eq. (28), we obtain

$$\begin{aligned} p_r(x) &= E_{rr}(x)\cos\Phi_{in} + E_{rt}(x)\sin\Phi_{in} \\ &= \sin^2\rho\cos\Phi_{in} + q(\Phi_{in}, \rho)\cos\rho\cos y, \quad \text{and} \\ p_t(x) &= E_{tr}(x)\cos\Phi_{in} + E_{tt}(x)\sin\Phi_{in} \\ &= -q(\Phi_{in}, \rho)\sin y, \end{aligned} \tag{56}$$

where $y = x - \zeta$ [see also Eq. (41)]. The predicted dependence of $p_{rt}(x)$ on the initial spin-precession phase Φ_{in} is shown in Fig. 5. For the exact resonance condition, $\cos\rho = 0$, we have

$$\begin{aligned} p_r(x) &= \cos\Phi_{in}, \\ p_t(x) &= \sin\Phi_{in}\cos x, \quad \text{and} \\ p_{rt}(x) &= \sqrt{\cos^2\Phi_{in} + \sin^2\Phi_{in}\cos^2 x}. \end{aligned} \tag{57}$$

This is yet another illustration of the emergence of the spectator radial polarization component p_r, which is immune to the rf-driven spin rotations and of the appearance of the active tangential polarization p_t, which is the partner component of the vertical polarization [see Eq. (42)].

The envelope $p_{rt}(x)$ is a smooth function of x with minima at $x_4 = \pi/2$ and $x_5 = \pi/2 + \pi$, and the maxima, $p_{rt} = 1$, at $x_3 = \pi$ and at the end points $x_1 = 0$ and $x_2 = 2\pi$. These features are evident from Fig. 3, since $p_{rt} = (1 - p_s^2)^{1/2}$.

We recall that the result from Eq. (48) for the continuous operation of the WF beginning with pure vertical polarization, shown in Fig. 3, was symmetric with respect to the substitution $x \Leftrightarrow 2\pi - x$. This symmetry is manifestly broken for nonvanishing values of Φ_{in} and $\cos\rho$ [see Eq. (40)], and we obtain

$$\begin{aligned} &p_{rt}^2(x) - p_{rt}^2(2\pi - x) = p_s^2(2\pi - x) - p_s^2(x) \\ &= 4\sin\Phi_{in}\cos\Phi_{in}\sin^2\rho\cos\rho\sin x(1 - \cos x). \end{aligned} \tag{58}$$

For finite ζ, one rather has an invariance of $p_{rt}(x)$ with respect to the interchange $x - \zeta \Leftrightarrow 2\pi - (x - \zeta)$ within the shifted symmetric interval $[\zeta, 2\pi + \zeta]$ [see the related discussion of Eq. (40)].

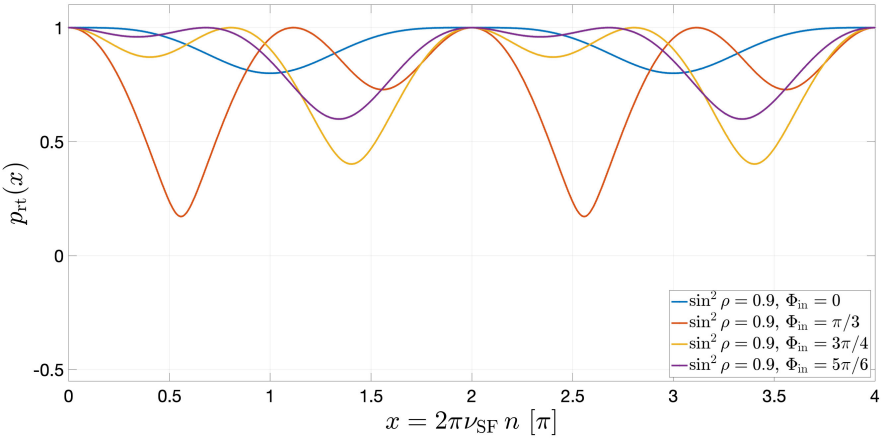

FIG. 5. Pattern of the x dependence of the horizontal polarization envelope $p_{\rm rt}$, which evolves from the initial horizontal polarization with different initial spin precession phases $\Phi_{\rm in}$. Within the interval $[0, 2\pi]$, the left-right symmetry of the envelope polarization at $\Phi_{\rm in} = 0, \pi$ is broken at $0 < \Phi_{\rm in} < \pi$ [see Eq. (58)]. However, the left-right symmetry is recovered within the symmetric period $[\zeta, 2\pi + \zeta]$, see the discussion of symmetry properties of Eq. (40).

2. *Phase of in-plane polarization envelope for pure radial and longitudinal initial polarizations*

The motion of the phase $\phi(x)$ of the envelope $\vec{p}_{\rm rt}$ is quite sensitive to the initial phase $\Phi_{\rm in}$ and the detuning angle ρ. It is sufficient to treat the case $\cos\rho \geq 0$, an extension of the results to $\cos\rho < 0$ is straightforward.

We start from Eq. (56) with the pure radial initial polarization case of $\Phi_{\rm in} = 0$, when $p_{\rm r}(x) = \sin^2\rho + \cos^2\rho\cos x$ and $p_{\rm t}(x) = -\cos\rho\sin x$. The results are shown in Fig. 6. First of all, $\phi(x)$ is antisymmetric with respect to $x \Leftrightarrow 2\pi - x$. Second, for all detuning angles we find $\phi(x) = \pi/2$ at $x = 0, \pi, 2\pi, \ldots$ Third, $\cos\phi(x_1) = -{\rm sgn}(\cos\rho\sin x_1) = \pm 1$, i.e., $\phi_1 = 0, \pi$, can be reached only if $p_{\rm r}(x_1) = 0$, i.e., at

$$\cos x_1 = -\tan^2\rho, \tag{59}$$

which is only possible for $\cos^2\rho \geq ½$.

In the vicinity of pointed tips at $|\cos(x_1) = 1$, we have $p_r(x) = -\cos^2\rho\,\sin x_1 \cdot (x - x_1)$ and

$$\begin{aligned} |\cos\phi(x)| &= 1 - \frac{1}{2}[\phi(x) - \phi(x_1)]^2 \\ &= \frac{1}{\sqrt{1 + \cos^2\rho(x - x_1)^2}} \\ &= 1 - \frac{1}{2}\cos^2\rho(x - x_1)^2, \end{aligned} \tag{60}$$

which yields the slope

$$\phi(x) - \phi_1 = \pm|\cos\rho||x - x_1|. \tag{61}$$

Note that the magnitude of the slope at the tip, $|\cos\rho|$, varies from $1/\sqrt{2}$ to 1.

In the opposite case of $\cos^2\rho < ½$, we have $0 < \phi(x) < \pi$. Locations of the extrema of $\phi(x)$ are roots of the equation $(\cos\psi(x))' = 0$, which takes the form

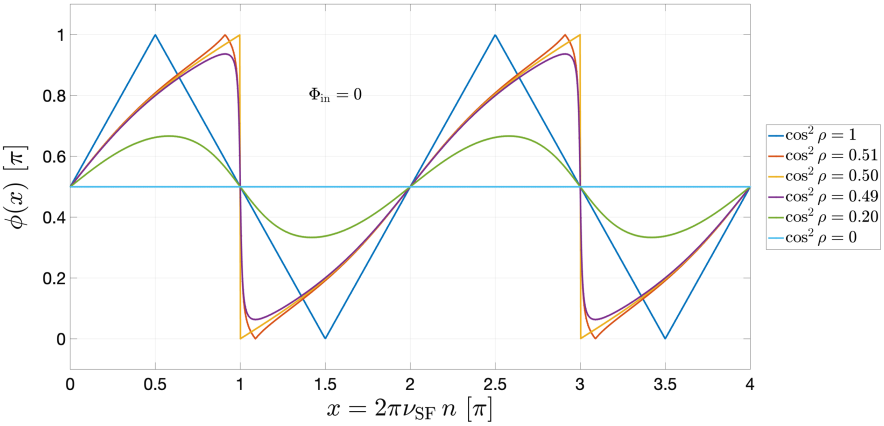

FIG. 6. Phase motion of the horizontal polarization envelope for $\Phi_{\rm in} = 0$ as predicted by Eq. (45). The full phase swing of $\phi_{\rm max} - \phi_{\rm min} = \pi$ is reached only for $\cos^2\rho \geq ½$, when $\phi(x)$ exhibits a pointed tip with the slope $\pm|\cos\rho|$. The phase motion evolves into the phase jump for the transition detuning, $\cos^2\rho \to ½$.

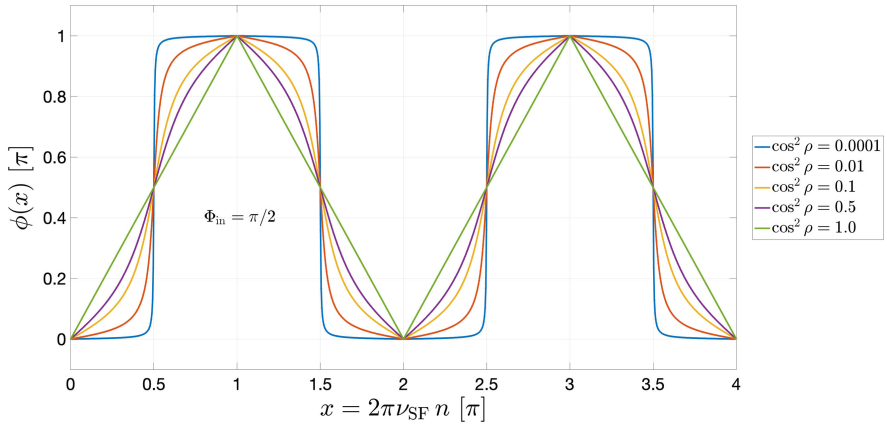

FIG. 7. Phase motion of the horizontal polarization envelope for $\Phi_{in} = \pi/2$ as predicted by Eq. (45). In the limit of $\cos\rho \to 0$, the phase motion evolves into the phase jumps and the central bumps at $x = \pi$ and 3π exhibit a rectangular shape.

$$\cos x + \sin^2\rho\cos^2\rho(1 - \cos x)^2 = 0 \tag{62}$$

and yields the root $\cos x = -\cot^2\rho$. The resulting phase span equals

$$\phi_{max} - \phi_{min} = 2\arccos|\cot\rho|. \tag{63}$$

With approach to the boundary of the two regimes, $\cos^2\rho \to ½$, the phase motion evolves into the phase jump at $x = \pi, 3\pi, \ldots$

The next interesting case is the pure tangential initial polarization, when

$$\cos\phi(x) = \frac{\mathrm{sgn}(\cos x)}{\sqrt{1 + \cos^2\rho\tan^2 x}}. \tag{64}$$

The corresponding results are presented in Fig. 7. The phase $\phi(x)$ is symmetric with respect to $x \Leftrightarrow 2\pi - x$ and the phase swing $\phi_{max} - \phi_{min} = \pi$ for all ρ. It exhibits pointed tips at $x = x_1$, when $\tan^2 x_1 = 0$, i.e., when $\phi(x_1) = 0$ for $x_1 = 0, 2\pi, \ldots$ and when $\phi(x_1) = \pi$ for $x_1 = \pi, 3\pi, \ldots$. In the vicinity of the pointed tip at $x = x_1$, the phase motion is given by

$$\phi_1 - \phi(x) = \pm|\cos\rho| \cdot |x - x_1|, \tag{65}$$

yielding exactly the same slope as in Eq. (61). The only distinction to the case of $\Phi_{in} = 0$ is that here $|\cos\rho| \le 1/\sqrt{2}$. Note that $\phi(\pi/2) = \pi/2$ and at $|\cos\rho| \ll 1$, the phase $\phi(x)$ passes $\pi/2$ steeply in the narrow range of $|x - \pi/2| < |\cos\rho|$. This steep variation of $\phi(x)$ about $x = \pi/2$ tends to a step function as $|\cos\rho| \to 0$ in the fashion discussed in Sec. IV E.

3. Evolution of the phase of in-plane polarization envelope for generic orientation of the initial polarization

The analysis is based on Eqs. (59) and (45). The salient features of $\phi(x)$ for generic Φ_{in} are illustrated in Fig. 8 for the example that $\Phi_{in} = \pi/4$. To start with, at $x = 0$ and $x = 2\pi$, Eq. (56) implies that

$$\phi(0) = \phi(2\pi) = \frac{\pi}{2} - \Phi_{in} \tag{66}$$

independent of the detuning parameter ρ.

The subsequent analytic discussion is most conveniently performed in terms of the variables $y = x - \zeta(\Phi_{in}, \rho)$ and $q(\Phi_{in}, \rho)$ [see Eqs. (41) and (56)]. A major finding is that the same universal slope at the tip, $\pm|\cos\rho|$, persists for all Φ_{in}. Indeed, according to Eq. (56), we have $p_r(x) = 0$ at

$$\cos y_1 = -\frac{\sin^2\rho\cos\Phi_{in}}{q(\Phi_{in}, \rho)\cos\rho}. \tag{67}$$

This solution is only possible if

$$\cos^2\rho \ge \cos^2\rho_m = \frac{\cos^2\Phi_{in}}{1 + \cos^2\Phi_{in}}, \tag{68}$$

where ρ_m denotes the boundary detuning angle for which the solution (67) does still exist.

In close similarity to the case $\Phi_{in} = 0$, shown in Fig. 6, the phase $\phi(x)$ exhibits pointed tips $x_1 = y_1 + \zeta$. In the vicinity of the tips, we have

$$\begin{aligned} p_r(x) &= -q(\Phi_{in}, \rho)\cos\rho\sin y_1 \cdot (x - x_1) \\ &= p_t(x_1)\cos\rho\sin y_1 \cdot (x - x_1), \end{aligned} \tag{69}$$

which entails

$$\cos\phi(x) = \frac{\mathrm{sgn}(\cos x)}{\sqrt{1 + \cos^2\rho(x - x_1)^2}}, \tag{70}$$

and we recovered Eq. (60) and the familiar slope $\pm\cos\rho$ at the pointed tips.

In the evaluation of the phase span at $\cos^2\rho \le \cos^2\rho_m$, we follow the procedure developed for the case of $\Phi_{in} = 0$.

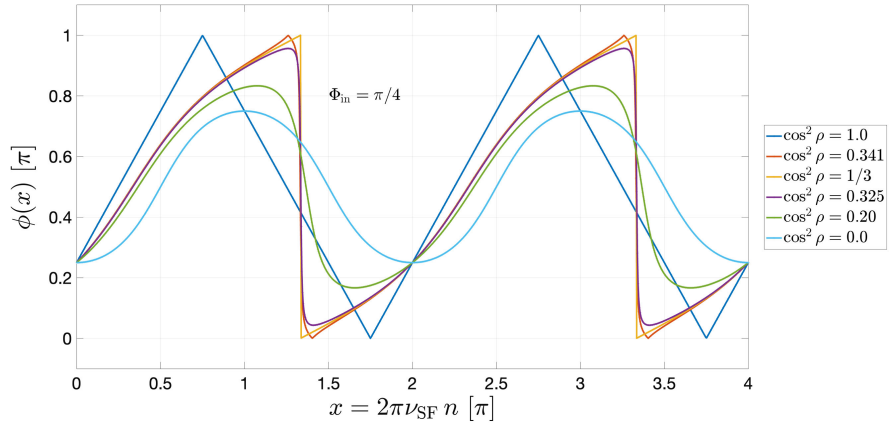

FIG. 8. Phase motion of the horizontal polarization envelope for $\Phi_{\rm in} = \pi/4$, as predicted by Eq. (45). For $\cos^2\rho \geq \cos^2\rho_m = 1/3$ [see Eq. (68)], the pattern of the phase motion resembles that for $\Phi_{\rm in} = 0$ depicted in Fig. 6. The phase jump for $\cos^2\rho = \cos^2\rho_m$ is located at $x = x_m = 4\pi/3$, as predicted by Eq. (75). In contrast to the case of $\Phi_{\rm in} = 0$ in Fig. 6, the phase motion for $\cos^2\rho < \cos^2\rho_m$ has no symmetry center.

The phase extrema are roots of the equation $(\cos\phi(x_m))' = 0$, which takes the form [here below $q = q(\Phi_{\rm in}, \rho)$]

$$\cos^2 y + 2w\,\cos y + 1 = 0, \tag{71}$$

with the roots

$$\cos y_\pm = w \pm \sqrt{w^2 - 1}, \tag{72}$$

where

$$w = \frac{\sin^2\rho(q^2 + \cos^2\rho\cos^2\Phi_{\rm in}) - 1}{2q\sin^2\rho\,\cos\rho\cos\Phi_{\rm in}}. \tag{73}$$

Solutions of the above equation exist for $w^2 \geq 1$. It is easy to check that the boundary case, $w = 1$, corresponds to the exact equality in the condition in Eq. (68). Subject to the constraint $|\cos y_\pm| \leq 1$, the admissible roots are $\cos y_-$ at $w \geq 1$, and $\cos y_+$ at $w \leq -1$, and the two branches are related by $\cos y_-(w) = -\cos y_+(-w)$.

Now, we focus on the boundary case $\cos\rho = \cos\rho_{\rm m} > 0$. According to Eq. (56), $p_{\rm t}(x)$ changes sign at $y = \pi$, and we encounter the by now familiar phase jump depicted in Fig. 6. Upon some algebra, we find

$$\cos\zeta(\Phi_{\rm in}, \rho_m) = \cos^2\Phi_{\rm in}, \tag{74}$$

which in our case $\Phi_{\rm in} = \pi/4$ entails $\zeta(\Phi_{\rm in}, \rho_m) = \pi/3$, and we predict

$$x_m = \pi + \arccos\left(\cos^2(\Phi_{\rm in})\right) = \frac{4}{3}\pi, \tag{75}$$

in perfect agreement with the numerical results shown in Fig. 8.

As we observed in Sec. IV F, a finite initial phase $\Phi_{\rm in}$ introduces an asymmetry with respect to $x \Leftrightarrow 2\pi - x$. The symmetry is restored in the exceptional case of $\cos\rho = 0$ [see Eq. (58)], when we predict $\phi(x = \pi) = 3\pi/4$ in agreement with the numerical results shown in Fig. 8.

Finally, we consider the case of $\Phi_{\rm in} = -\pi/4$. The corresponding phase motion is shown in Fig. 9. First, according to Eq. (66), we get

$$\phi(0) = \phi(2\pi) = \frac{\pi}{2} - \Phi_{\rm in} = \frac{3}{4}\pi, \tag{76}$$

Second, according to Eq. (41), now we must take a branch $\zeta = -\arccos\left(\cos^2(\Phi_{\rm in})\right)$. As far as the x dependence of the phase $\phi(x)$ is concerned, a chain of substitutions

$$\begin{aligned} y = x - \zeta|_{\pi/2} &\Rightarrow x - \zeta|_{-\pi/2} = x + \zeta|_{\pi/2} \\ &\Rightarrow \tilde{y} = -[(-x) - \zeta|_{\pi/2}], \end{aligned} \tag{77}$$

amounts to the up-down and left-right reflections, i.e., inversion of the x axis accompanied by the shift by 2π, and simultaneous phase inversion $\phi(x) \Rightarrow \pi - \phi(x)$.

4. Summary on the in-plane polarization phase

We found a very rich pattern of in-plane envelope phase motion as a function of detuning and initial spin phase. Still, there are certain universal features of the graphs shown in Figs. 6–9, which are worth of emphasis. Irrespective of $\Phi_{\rm in}$, in all graphs, the envelope phase exhibits the phase jump by π with the known $\Phi_{\rm in}$ dependence of the location of the jump. The same is true for the continuous spin rotation [see Fig. 4], although this case has certain exceptional features to be discussed below. For nonvanishing detuning, $\phi(x)$ exhibits pointed tips with a universal slope equal to $\pm\cos\rho$ at the tip, irrespective of the initial spin phase, while in Fig. 4, the related slope equals $|\cos\rho|/2$. Finally, the phase continuity condition $\phi(x = 0) = \phi(x = 2\pi)$ holds for all $\Phi_{\rm in}$ with the detuning-independent $\phi(0)$, again with the exception of Fig. 4.

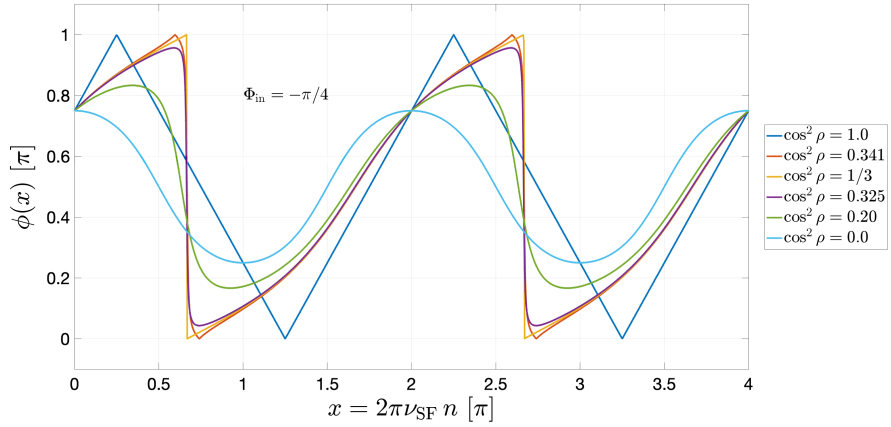

FIG. 9. Phase motion for $\Phi_{\rm in} = -\pi/4$ as predicted by Eq. (45). For $\cos^2\rho \geq \cos^2\rho_m = 1/3$ [see Eq. (68)], the pattern of the phase motion resembles that for $\Phi_{\rm in} = 0$ depicted in Fig. 6. The phase jump for $\cos^2\rho = \cos^2\rho_m$ is located at $x = x_m = 2\pi/3$, and, as predicted by Eq. (75), after reflections is described by Eq. (77).

Regarding the pointed tips, according to Eq. (68), they persist for a finite range of detuning, apart from the exceptional cases $\Phi_{\rm in} = \pm\pi/2$, when the tips for all ρ share identical locations at $x = 0, \pi, 2\pi, \ldots$

The WF-driven *continuous* evolution from the pure vertical initial polarization is distinct from the generic three-stage evolution used in actual JEDI experiments. As explained in Sec. IV B, here WF operates in the capacity of the spin rotator in stage I and continuous on to stage III at one and the same detuning angle ρ. Specifically, the rotation of the polarization into the horizontal plane happens at $\cos x_0(\rho) = -\cot^2\rho$ [see Eq. (37)]. In the spirit of generic three-stage process, this instant can be viewed as a start of stage III with the initial phase $\Phi_{\rm in}$ defined by

$$\cos\Phi_{\rm in} = p_{\rm r}(x_0) = \cot\rho,$$
$$\sin\Phi_{\rm in} = p_{\rm t}(x_0) = \mathrm{sgn}(\sin\rho)\sqrt{1-\cot^2\rho}. \qquad (78)$$

Our convention for stage III is that the envelope evolution phase starts with $x = 0$. Evidently, the further evolution of $p_{\rm r,t}(x)$ will be still described by Eq. (47) subject to the trivial substitution $x \to x + x_0(\rho)$. This way in Fig. 4, we lumped together the detuning dependence of $\phi(x)$ for a very special subset of initial phases $\Phi_{\rm in}(\rho)$ as opposed to the ρ-independent initial phase in other cases. This distinctive feature of continuous evolution is behind the ρ-independent phase jump at 0, 2π, 4π, …, and the degeneracy of the tip and jump locations, and a phase slope at the tip, $\frac{1}{2}\cos\rho$, which is half of that in the generic case.

The above analysis suggests that the phase of the envelope of the horizontal polarization has a great potential for the diagnostics of the rf-driven spin dynamics (see also early considerations in Ref. [25]). We demonstrated a remarkably strong sensitivity of the phase motion to the initial phase of the horizontal spins and to the detuning of the spin precession frequency. This phase remained the as yet poorly explored feature of the rf-driven spin dynamics in storage rings, and we make a point that variations of the dependence of this phase with respect to time may prove as a good indicator of the stability of the detuning during the cycle, or as an indicator for the lack or the presence of unwanted phase walks.

V. SPIN DECOHERENCE INCORPORATED

A. Recovering the spectator polarization

As a prelude to further discussion of the spin decoherence effects, we observe that the envelope evolution matrix in Eq. (28) can be cast in the form

$$\mathbf{E}(x) = \begin{pmatrix} \sin^2\rho + \cos^2\rho\cos x & \cos\rho\sin\rho(1-\cos x) & \cos\rho\sin x \\ \cos\rho\sin\rho(1-\cos x) & \cos^2\rho + \sin^2\rho\cos x & -\sin\rho\sin x \\ -\cos\rho\sin x & \sin\rho\sin x & \cos x \end{pmatrix}$$
$$= \begin{pmatrix} \sin\rho & -\cos\rho & 0 \\ \cos\rho & \sin\rho & 0 \\ 0 & 0 & 1 \end{pmatrix} \cdot \begin{pmatrix} 1 & 0 & 0 \\ 0 & \cos x & -\sin x \\ 0 & \sin x & \cos x \end{pmatrix} \cdot \begin{pmatrix} \sin\rho & \cos\rho & 0 \\ -\cos\rho & \sin\rho & 0 \\ 0 & 0 & 1 \end{pmatrix}, \qquad (79)$$

which amounts to the rotation of coordinates such that the vector $\vec{m}$ of Eq. (29) plays now the role of $\vec{e}_s$ in the case of idle precessions. In this new reference frame, the matrix in Eq. (28) stems from the initial block-diagonal matrix $\mathbf{E}_0(x)$ of Eq. (17), which features the spectator polarization. This observation serves as a crucial guidance to link spin evolution to decoherence effects.

As a matter of fact, the presence of the hidden spectator component could have been directly guessed from the original envelope rotation matrix of Eq. (28). Indeed, besides the manifestly rf-driven terms $\propto \sin x$ and $\propto \cos x$, the four matrix elements of $\mathbf{E}(x)$ do components $\sin^2\rho$ in $E_{rr}(x)$, $\cos^2\rho$ in $E_{ss}(x)$, and $\cos\rho\sin\rho$ in $E_{rs}(x)$ and $E_{sr}(x)$, which do not participate in the spin-flip process.

B. Ansatz of exponential decoherence of the in-plane polarization

1. Damped spin rotations

The JEDI studies of spin decoherence have revealed [11] an enhancement of the spin-coherence time by the fine tuning of families of sextupole magnets to zero chromaticity to reduce the spread of spin tunes in the beam caused by orbit lengthening due to betatron oscillations [10]. In the spirit of the Bloch approach to NMR [4], we present here the *ad hoc* treatment of the residual spin decoherence in terms of the exponential attenuation of the in-plane polarization $\vec{S}(n)$ of an ensemble (bunch) of particles and preservation of the vertical polarization in the idle precession regime, as suggested by the experimental observations [17]. Correspondingly, the master equation (3) will be modified to yield

$$\vec{S}(n) = \mathbf{R}_{\rm WF}(n)\mathbf{R}_\Gamma\mathbf{R}_s(\theta_{\rm WF})\vec{S}(n-1), \tag{80}$$

where

$$\mathbf{R}_\Gamma = \begin{pmatrix} 1-\Gamma & 0 & 0 \\ 0 & 1 & 0 \\ 0 & 0 & 1-\Gamma \end{pmatrix} = \mathbf{1} + \mathbf{W}_\Gamma \tag{81}$$

describes the attenuation per turn, where in terms of the spin coherence time $\tau_{\rm SCT}$, Γ is given by

$$\Gamma = \frac{1}{f_{\rm rev}\tau_{\rm SCT}}. \tag{82}$$

We shall also use the small decoherence parameter

$$Q = \frac{\Gamma}{4\pi\nu_{\rm SF}}, \tag{83}$$

which is defined such that $\Gamma n = 2Qx$.

2. Sequential Bogoliubov-Krylov averaging

Anticipating the sequential BK averaging, we seek for a solution of the master equation (80) of the form

$$\vec{S}(n) = \mathbf{R}_s(n\theta_{\rm WF})\mathbf{E}_0(n)\vec{g}(n), \tag{84}$$

so that $\vec{g}(n)$ will embody the impact of the spin decoherence on the earlier defined spin envelope: $\vec{p}(n) = \mathbf{E}_0(n)\vec{g}(n)$. Then the master equation for $\vec{g}(n)$ reads

$$\vec{g}(n) = \mathbf{E}_0^{-1}(n)\mathbf{R}_s^{-1}(n\theta_{\rm WF})\mathbf{R}_{\rm WF}(n)\mathbf{R}_s(n\theta_{\rm WF})\mathbf{R}_\Gamma\mathbf{E}_0(n-1)\vec{g}(n-1). \tag{85}$$

The first stage of the BK averaging over spin precession yields

$$\langle \mathbf{R}_s^{-1}(n\theta_{\rm WF})\mathbf{R}_{\rm WF}(n)\mathbf{R}_s(n\theta_{\rm WF})\rangle = \mathbf{E}_0(1). \tag{86}$$

Next, we perform the BK averaging over spin flips that are fast compared to the spin damping:

$$\mathbf{U}_\Gamma = \langle \mathbf{E}_0^{-1}(n-1)\mathbf{W}_\Gamma\mathbf{E}_0(n-1)\rangle = \Gamma\left\langle \begin{pmatrix} 1 & 0 & 0 \\ 0 & \sin^2 x & 0 \\ 0 & 0 & \cos^2 x \end{pmatrix}\right\rangle = -\Gamma\begin{pmatrix} 1 & 0 & 0 \\ 0 & \frac{1}{2} & 0 \\ 0 & 0 & \frac{1}{2} \end{pmatrix}. \tag{87}$$

The corresponding solution of Eq. (85) is given by

$$\vec{g}(n) = \mathbf{E}_\Gamma(n)\vec{p}(0) = \exp(\mathbf{U}_\Gamma n)\vec{p}(0), \tag{88}$$

with

$$\mathbf{E}_\Gamma(x) = \begin{pmatrix} \exp(-2Qx) & 0 & 0 \\ 0 & \exp(-Qx) & 0 \\ 0 & 0 & \exp(-Qx) \end{pmatrix}. \tag{89}$$

While the idly precessing spectator component decoheres $\propto \exp(-2Qx)$, the vertical and the in-plane active polarizations decohere at half this rate, $\propto \exp(-Qx)$. Indeed, the polarization decoheres when it is in the rt-plane, while the attenuation of the upward or downward polarization is negligibly weak on the time scale of τ_{SCT} [17]. The corresponding damped envelope evolution reads $\vec{p}(x) = \mathbf{E}_{\mathrm{D}}(x)\vec{p}(0)$ with the SF matrix

$$\mathbf{E}_{\mathrm{D}}(x) = \mathbf{E}_0(x)\mathbf{E}_\Gamma(x) = \begin{pmatrix} \exp(-2Qx) & 0 & 0 \\ 0 & \exp(-Qx)\cos x & -\exp(-Qx)\sin x \\ 0 & \exp(-Qx)\sin x & \exp(-Qx)\cos x \end{pmatrix}, \tag{90}$$

which replaces $\mathbf{E}_0(x)$ in Eq. (79) with the result

$$\mathbf{E}_{\mathrm{exp}}(x) = \begin{pmatrix} e^{-2Qx}\sin^2\rho + e^{-Qx}\cos^2\rho\cos x & \cos\rho\sin\rho(e^{-2Qx} - e^{-Qx}\cos x) & e^{-Qx}\cos\rho\sin x \\ -\cos\rho\sin\rho(e^{-2Qx} - e^{-Qx}\cos x) & e^{-2Qx}\cos^2\rho + e^{-Qx}\sin^2\rho\cos x & -e^{-Qx}\sin\rho\sin x \\ -e^{-Qx}\cos\rho\sin x & e^{-Qx}\sin\rho\sin x & e^{-Qx}\cos x \end{pmatrix}. \tag{91}$$

In this purely phenomenological approach, there is no direct link between the attenuation and the SF tune [44].

C. Spin decoherence by synchrotron motion

1. Spread of synchrotron oscillation amplitudes

So far, we considered only central particles in the bunch. The synchrotron oscillations (SO) with frequency f_{sy} modulate the particle momentum and the spin tune and are endemic in storage rings. The emerging oscillating detuning between WF and spin precession is a well-defined dynamical mechanism of spin decoherence, and here we treat it as the leading one, supposing that the betatron oscillation effects have been taken care of by fine tuning of the sextupole families. We follow the technique of an earlier study [45] and extend these considerations.

Oscillations of particles around the center of the bunch can be evaluated using the time distribution of the events recorded in the polarimeter. Following Ref. [29], it is convenient to represent the synchrotron motion and longitudinal profile of the bunch in terms of a fractional phase of the beam revolution, ϕ_{rev},

$$\phi = \phi_{\mathrm{rev}} - 2\pi n, \qquad \phi \in [0, 2\pi]. \tag{92}$$

In the further discussion, the synchrotron motion for an individual particle is defined with respect to a center of the bunch:

$$\phi = a\cos(2\pi\nu_{\mathrm{sy}} f_{\mathrm{sy}} t + \lambda), \tag{93}$$

where $\nu_{\mathrm{sy}} = f_{\mathrm{sy}}/f_{\mathrm{rev}}$ is the synchrotron tune, and $\lambda \in [0, 2\pi]$ is the individual particle's random phase.

The one-particle contribution to the longitudinal density of the bunch $N(\phi)$, as determined from the time distribution of events in the polarimeter, is inversely proportional to the modulus of the SO velocity v_{sy}. For harmonic oscillations as in Eq. (93), we can relate the velocity to the phase ϕ via

$$\begin{aligned} v_{\mathrm{sy}} &= 2\pi f_{\mathrm{sy}} a |\sin(2\pi\nu_{\mathrm{sy}} f_{\mathrm{rev}} t + \lambda)| \\ &= 2\pi f_{\mathrm{sy}}\sqrt{a^2 - \phi^2}, \end{aligned} \tag{94}$$

so that the one-particle density of the bunch, $N(\phi)$, receives contributions only from particles with synchrotron amplitudes $a > \phi$ and is related by the Abel equation (transform) to the synchrotron amplitude distribution function $F(a)$ through

$$N(\phi) = \frac{1}{\pi}\int_\phi^\infty \frac{\mathrm{d}aF(a)}{\sqrt{a^2 - \phi^2}}. \tag{95}$$

Taking advantage of the experimental knowledge of $N(\phi)$, we invoke the inverse Abel transform:

$$F(a) = -2a\int_a^\infty \frac{\mathrm{d}\phi N'(\phi)}{\sqrt{\phi^2 - a^2}}, \tag{96}$$

which relates the longitudinal SO velocity distribution to the derivative of the longitudinal spatial density of the bunch. For the Gaussian approximation

$$N(\phi) \propto \exp(-\phi^2/2\sigma_{\mathrm{sy}}^2), \tag{97}$$

which represents well the experimentally observed longitudinal profile of the bunch [29], the inverse Abel transform in Eq. (96) yields analytic solutions in the form of the Rayleigh distribution [46]:

$$F(a) = \frac{a}{\sigma_{\mathrm{sy}}^2}\exp\left(-\frac{a^2}{2\sigma_{\mathrm{sy}}^2}\right). \tag{98}$$

The synchrotron modulation of the particle momentum $\Delta p(n)$ and the revolution period $\Delta T(n)$ are related by the slip factor η

$$\frac{\Delta T}{T} = \frac{\Delta\phi(n)}{2\pi} = \eta \cdot \frac{\Delta p(n)}{p}, \tag{99}$$

where η

$$\eta = \frac{1}{\gamma^2} - \frac{1}{\gamma_{\rm tr}^2}, \tag{100}$$

and $\gamma_{\rm tr}$ is the transition gamma factor [47]. In Eq. (99), we introduced $\Delta\phi(n)$, an angular advance (retardation) of a particle per revolution n oscillating with time $\propto \cos(2\pi\nu_{\rm sy} f_{\rm rev} t)$. These one-turn synchrotron phase shifts sum precisely to the ϕ defined above with an amplitude larger by the large factor $(2\pi\nu_{\rm sy})^{-1}$ than that of $\Delta\phi(n)$. Averaging over the ensemble of particles yields the simple relationship

$$\sigma_{\rm sy} = \langle\phi^2\rangle^{1/2} = \frac{\eta}{\nu_{\rm sy}} \left\langle \frac{(\Delta p)^2}{p^2} \right\rangle^{1/2}. \tag{101}$$

The SOs generate a cumulative shift of the spin precession phase, $\Delta\theta_{\rm s}(n) = \theta_{\rm s}(n) - \theta_{\rm s} n$, which is a sum of shifts $\delta\theta_{\rm s}(n)$ per turn:

$$\begin{aligned} \delta\theta_{\rm s}(n) &= 2\pi G\delta\gamma = 2\pi G\gamma\beta^2 \frac{\Delta p(n)}{p}, \\ \Delta\theta_{\rm s}(n) &= \sum_{k=1}^{n} \delta\theta_{\rm s}(k) = \xi\psi_{\rm sy} \sin(2\pi\nu_{\rm sy} n + \lambda), \\ \psi_{\rm sy} &= \sqrt{2} G\gamma\beta^2 \frac{\sigma_{\rm sy}}{|\eta|}, \end{aligned} \tag{102}$$

where ξ is a convenient phase-slip relative amplitude with the distribution function:

$$F(\xi) = 2\xi \exp(-\xi^2), \tag{103}$$

and normalization $\langle\xi^2\rangle = 1$ [cf., Eq. (98)].

The modulation ΔT of the revolution time results in the corresponding SO-driven slip of the WF phase:

$$\begin{aligned} \Delta\theta_{\rm WF}(n) &= \frac{f_{\rm WF}}{f_{\rm s}} \cdot \frac{\eta}{\beta^2} \Delta\theta_{\rm s} = C_{\rm WF} \Delta\theta_{\rm s}(n), \\ C_{\rm WF} &= 1 + \frac{K}{G\gamma}, \end{aligned} \tag{104}$$

which will show up in the spin-flip dynamics [48].

2. Master equation for the spin envelope

It suffices to consider the case of the exact resonance for the central particle, $f_{\rm WF} = f_{\rm s}$, i.e., $\theta_{\rm s} = \theta_{\rm WF}$ [49]. The SO-modified one-turn spin transfer will be given by

$$\vec{S}(n) = \mathbf{R}_{\rm WF}(n)\mathbf{R}_{\rm s}(\theta_{\rm s} + \delta\theta_{\rm s}(n))\vec{S}(n-1). \tag{105}$$

Bearing in mind the subsequent Fourier analysis of the in-plane polarization, we stick to the definition of the spin envelope via Eq. (9), i.e., we define the envelopes in the reference frame co-rotating with the fixed angular velocity $\omega_{\rm WF}$.

The simple rotations in Eq. (105) preserve the magnitude of the polarization of individual particles. However, experimentally one measures the average polarization of an ensemble of particles with a typical observation time that is much longer than the SO period. This averaging over the ensemble leads to spin decoherence and depolarization.

As an exercise, we first treat the simplest case of the pure idle precession of the in-plane polarization. Here the determination of the envelope $p_{\rm rt}$ by the Fourier analysis amounts to the projection of the polarization on the unit vector rotating with fixed frequency $f_{\rm WF}$. For an individual particle, the average over the SO period equals

$$\begin{aligned} p_{\rm rt}(\xi) &= \langle \exp(i\Delta\theta_{\rm s}(n)) \rangle \\ &= \langle \cos(\xi C_{\rm WF}\psi_{\rm sy} \sin(2\pi\nu_{\rm sy} n + \lambda)) \rangle \\ &= J_0(\xi\psi_{\rm sy}), \end{aligned} \tag{106}$$

and the average of the Bessel function over the ensemble of particles in the bunch is

$$\begin{aligned} p_{\rm rt} &= \int_0^\infty 2\xi \exp(-\xi^2) J_0(\xi\psi_{\rm sy}) d\xi \\ &= \exp\left(-\frac{1}{4}\psi_{\rm sy}^2\right) \approx 1 - \frac{1}{4}\psi_{\rm sy}^2. \end{aligned} \tag{107}$$

This weak time-independent reduction of $p_{\rm rt}$ is of rather academic relevance, because the instantaneous injection of horizontal polarization into the ring is technically impossible. Equally impossible is polarimetry with sufficiently large statistics at times much shorter than the SO period. Consequently, in practice, the suppression in Eq. (107) is reabsorbed in the definition of the magnitude of the initial in-plane polarization as determined experimentally by polarimetry prior to switching on the rf spin rotator.

Now, we generalize the master equation (26) with allowance for SOs:

$$\vec{p}(n) = \mathbf{R}_{\rm s}(-n\theta_{\rm WF})\mathbf{R}_{\rm WF}(n)\mathbf{R}_{\rm s}(\delta\theta_{\rm s}(n))\mathbf{R}_{\rm s}(n\theta_{\rm WF})\vec{p}(n-1). \tag{108}$$

Here, SOs enter via the slip of the spin phase per turn, $\delta\theta_{\rm s}(n)$, and the cumulative slip of the WF phase $\Delta\theta_{\rm WF}(n)$ in $\mathbf{R}_{\rm WF}(n)$. In the Fourier analysis, one is bound to sample trains of turns much longer than the SO period so that the detuning *per se* averages out to zero, $\langle\delta\theta_{\rm s}(n)\rangle = 0$, but we have already seen the nonvanishing SO effect even in the case of idle precession, see Eq. (107).

In the BK averaging over rapid spin precessions of the corresponding counterpart of the matrix in Eq. (13), we encounter

$$\langle \cos(\theta_{\rm WF} n)\cos(\theta_{\rm WF} n + C_{\rm WF}\Delta\theta_{\rm s}(n))\rangle \Rightarrow \frac{1}{2}\cos(C_{\rm WF}\Delta\theta_{\rm s}(n)),$$
$$\langle \sin(\theta_{\rm WF} n)\cos(\theta_{\rm WF} n + C_{\rm WF}\Delta\theta_{\rm s}(n))\rangle \Rightarrow -\frac{1}{2}\sin(C_{\rm WF}\Delta\theta_{\rm s}(n)), \tag{109}$$

and obtain

$$\mathbf{U}_{\rm SO}(n) = \begin{pmatrix} 0 & -\frac{1}{2}\chi_{\rm WF}\sin(C_{\rm WF}\Delta\theta_{\rm s}(n)) & \delta\theta_{\rm s}(n) \\ \frac{1}{2}\chi_{\rm WF}\sin(C_{\rm WF}\Delta\theta_{\rm s}(n)) & 0 & -\frac{1}{2}\chi_{\rm WF}\cos(C_{\rm WF}\Delta\theta_{\rm s}(n)) \\ -\delta\theta_{\rm s}(n) & \frac{1}{2}\chi_{\rm WF}\cos(C_{\rm WF}\Delta\theta_{\rm s}(n)) & 0 \end{pmatrix}. \tag{110}$$

The next stage is BK averaging over the period of SOs that are much faster than the envelope rotations:

$$\langle \cos(C_{\rm WF}\Delta\theta_{\rm s}(n))\rangle = J_0(\xi C_{\rm WF}\psi_{\rm sy}),$$
$$\langle \sin(C_{\rm WF}\Delta\theta_{\rm s}(n))\rangle = 0,$$
$$\langle \delta\theta_{\rm s}(n)\rangle = 0, \tag{111}$$

so that

$$\langle \mathbf{U}_{\rm SO}(n)\rangle = \frac{1}{2}\chi_{\rm WF} J_0(\xi C_{\rm WF}\psi_{\rm sy})\mathbf{U}, \tag{112}$$

with familiar matrix $\mathbf{U}$ of Eq. (13).

The emerging SO-driven reduction of the SF tune

$$\nu_{\rm SF} \Rightarrow \nu_{\rm SF}(\xi) = \nu_{\rm SF} J_0(\xi C_{\rm WF}\psi_{\rm sy}) \tag{113}$$

has a simple interpretation. Indeed,

$$\delta(n) = C_{\rm WF}\delta_{\rm s}(n) \tag{114}$$

is merely a running detuning parameter which oscillates slowly with the SO frequency. Considering Eqs. (32) and (29), this leads to a jitter of the envelope rotation axis $\vec{m}$ over the SO period, which will influence the spin-flip rate.

In the case of weak to moderate SO effects, we can approximate

$$1 - J_0(\xi C_{\rm WF}\psi_{\rm sy}) \approx Q_{\rm sy}\xi^2, \tag{115}$$

where

$$Q_{\rm sy} = \frac{1}{4}C_{\rm WF}^2\psi_{\rm sy}^2 = \frac{1}{2}(K+G\gamma)^2\sigma_{\rm sy}^2. \tag{116}$$

For instance, the bunch length measured in the JEDI pilot-bunch experiment [29] corresponds to $Q_{\rm sy} \approx 0.01$. Remarkably, the parameter $Q_{\rm sy}$ is uniquely encoded in terms of the squared angular length of the bunch. Deuterons have a small magnetic anomaly, $G = -0.1416$, and at intermediate energies, $Q_{\rm sy}$ exhibits a strong sensitivity on the sideband K, which is a good signature of the SO dominance model. For relativistic protons, the sensitivity to the side band is less strong, and $Q_{\rm sy}$ scales with $(\gamma\sigma_{\rm sy})^2$ [50].

3. Evaluation of synchrotron oscillation-driven spin decoherence of the bunch polarization

The above defined $Q_{\rm sy}$ is the principal parameter, which defines the SO-driven spread of the spin-flip tune in Eq. (113) and the spin-flip phase:

$$x \Rightarrow x(\xi) = xJ_0(\xi C_{\rm WF}\psi_{\rm sy}) \approx x - Q_{\rm sy}\xi^2 x, \tag{117}$$

where x is given by Eq. (30). The SO-driven decoherence is quantified by the expectation value over the ensemble of particles in the bunch, $\langle \mathbf{E}(x(\xi))\rangle_\xi$, with the weight function $F(\xi)$ of Eq. (103). We need to evaluate

$$\langle \exp(ix(\xi))\rangle_\xi = \exp(ix)\int_0^\infty d\xi F(\xi)\exp(-iQ_{\rm sy}\xi^2 x). \tag{118}$$

With the approximation in Eq. (115), we obtain

$$\langle \exp(ix(\xi))\rangle_\xi = \frac{\exp(ix)}{1+iQ_{\rm sy}x} = D(x)\exp(ix_{\rm sy}). \tag{119}$$

where the damping (depolarization) factor of the ensemble polarization equals

$$D(x) = \frac{1}{\sqrt{1+Q_{\rm sy}^2 x^2}}. \tag{120}$$

The spin-flip phase $x_{\rm sy}$ acquires a damping-related nonlinear walk:

$$x_{\rm sy} = x - \varphi_{\rm sy}(x), \quad \text{with}$$
$$\varphi_{\rm sy}(x) = \arctan(Q_{\rm sy}x). \tag{121}$$

The experimental results on the bunch length suggest $Q_{\rm sy} \ll 1$ [29].

The resulting counterpart of the envelope rotation matrix of Eq. (90) is given by

$$\mathbf{E}_{\mathrm{D}}^{(\mathrm{sy})}(x)=\begin{pmatrix}1 & 0 & 0\\ 0 & D(x)\cos x_{sy} & -D(x)\sin x_{\mathrm{sy}}\\ 0 & D(x)\sin x_{\mathrm{sy}} & D(x)\cos x_{\mathrm{sy}}\end{pmatrix}. \quad (122)$$

In the above derivation, the exact spin resonance was assumed for the central particles in the bunch.

Now, with reference to the representation from Eq. (79), a counterpart of the spin-flip matrix Eq. (91) for SO-driven detuning takes the form:

$$\mathbf{E}_{\mathrm{sy}}(x)=\begin{pmatrix}\sin^2\rho+D(x)\cos^2\rho\cos x_{\mathrm{sy}} & \cos\rho\sin\rho(1-D(x)\cos x_{\mathrm{sy}}) & D(x)\cos\rho\sin x_{\mathrm{sy}}\\ \cos\rho\sin\rho(1-D(x)\cos x_{\mathrm{sy}}) & \cos^2\rho+D(x)\sin^2\rho\cos x_{\mathrm{sy}} & -D(x)\sin\rho\sin x_{\mathrm{sy}}\\ -D(x)\cos\rho\sin x_{\mathrm{sy}} & D(x)\sin\rho\sin x_{\mathrm{sy}} & D(x)\cos x_{\mathrm{sy}}\end{pmatrix}. \quad (123)$$

The SO damping factor starts as $D(x)\approx 1-\frac{1}{2}Q_{\mathrm{sy}}^2x^2$ at $Q_{\mathrm{sy}}x\ll 1$, in contrast to $\exp(-Qx)\approx 1-Qx$ for the exponential Ansatz, while for large evolution times, the attenuation $D(x)\approx 1/(Q_{\mathrm{sy}}x)$ is slower than the exponential one. With the bunch and WF parameters of the pilot bunch experiment, the SO driven depolarization turned out to be still at the level of the experimental error bars [29].

A signature of the SO-dominated spin coherence time is that its scale is set by $Q_{\mathrm{sy}}x\sim 1$ and exhibits strong dependence on the SF frequency:

$$\tau_{\mathrm{SCT}}\sim\frac{1}{2\pi f_{\mathrm{SF}}Q_{\mathrm{sy}}}. \quad (124)$$

Finally, the synchrotron oscillations entail a nonlinear spin-flip phase walk $\varphi_{\mathrm{sy}}(x)$. It is an indispensable feature of the SO mechanism of spin decoherence, and it cannot be eliminated by the feedback process targeting the vanishing detuning. This phase walk $\varphi_{\mathrm{sy}}(x)$ entails the running SF tune:

$$\nu_{\mathrm{SF}}^{(\mathrm{sy})}(x)=\nu_{\mathrm{SF}}^{(\mathrm{sy})}\frac{dx_{\mathrm{sy}}(x)}{dx}=\nu_{\mathrm{SF}}^{(\mathrm{sy})}\left(1-\frac{Q_{\mathrm{sy}}}{1+Q_{\mathrm{sy}}^2x^2}\right), \quad (125)$$

where $\nu_{\mathrm{SF}}^{(\mathrm{sy})}$ is the constant spin-flip tune, which defines the principal spin-flip phase x and is given by Eqs. (31) and (33) (see further Sec. VIII).

The SO-mediated spin-flip matrix $\mathbf{E}_{\mathrm{sy}}(x_{\mathrm{sy}})$ differs in several aspects from the matrix of the exponential model $\mathbf{E}_{\mathrm{exp}}(x)$. In the SO mechanism, the time-dependent spin decoherence only takes place in the spin-flip process. In both scenarios, the magnitude of the polarization is not conserved, but in contrast to the exponential Bloch damping approach of Sec. V B [see Eq. (90)], the radial polarization of the precessing spectator does not decohere in the SO mechanism. Consequently, the interplay of vertical and horizontal polarizations, the evolution of the envelope and the motion of the phase of the horizontal polarization are different from those of the Bloch Ansatz and the spin-coherence-free case. We postpone the lengthy analysis of these changes to a future systematic investigation of the available experimental JEDI data on the evolution of the horizontal polarization.

D. Excursion on not compensated betatron oscillation effects

A strong enhancement of the spin coherence time by tuning the chromaticity, which suppresses orbit lengthening effects caused by betatron oscillations (BO), is well demonstrated experimentally [10–12]. Here, we comment on the possibility that the residual spin decoherence is an artifact of undercompensated BO effects. BO tunes are large, for example in COSY $\nu_{x,y}\approx 3.6$, some four orders of magnitude larger than the SO tune, yet the above treatment of SO effects can be extended to BOs as well. In fact, the prolongation of the orbit by BOs can be considered as a time-independent feature of individual particles. Its effect on the spin tune is proportional to the square of the BO amplitude:

$$\nu_{\mathrm{s}}(\xi)=(1-Q_\beta\xi^2)\nu_{\mathrm{s}}, \quad (126)$$

which is equivalent to a finite detuning of

$$\delta(\xi)=2\pi\nu_{\mathrm{WF}}Q_\beta\xi^2, \quad (127)$$

where ξ is the relative amplitude of the BOs with the distribution function $F(\xi)$ of Eq. (103). According to Refs. [10–12], by fine tuning the chromaticity, the BO parameter Q_{sy} could ideally be brought to zero.

We abstract from the dynamical considerations and comment here on the phenomenological consequences of the undercompensated BO effects. The most important point is a BO-dependent spread of the detuning, which results in a spread of SF tune. The small-δ expansion of the SF tune of Eq. (31) gives

$$\nu_{\mathrm{SF}}(\xi)=\nu_{\mathrm{SF}}^0\left(1+\frac{1}{2}Q_\beta\xi^4\right), \quad \text{where}$$
$$Q_\beta=Q_{\mathrm{sy}}^2\left(\frac{\nu_{\mathrm{WF}}}{\nu_{\mathrm{SF}}^0}\right)^2. \quad (128)$$

The BO correction to the SF tune starts with a term $\propto \xi^4$ compared to the $\propto \xi^2$ term in the SO Eq. (113), while the qualitative features are preserved.

Indeed, for the average over the ensemble, the BO-driven spread of the SF phase factor yields

$$\int_0^\infty d\xi F(\xi) \exp\left[i\frac{x}{2}Q_\beta \xi^4\right] = \frac{1}{\sqrt{1-i2Q_\beta x\rho_\beta(x)}} = D_\beta(x)\exp(i\varphi_\beta(x)), \quad (129)$$

with

$$D_\beta(x) = \{1+4Q_\beta^2 x^2 \rho_\beta^2(x)\}^{1/4},$$
$$\varphi_\beta(x) = \frac{1}{2}\arctan\left[2Q_\beta x\rho_\beta(x)\right],$$
$$\rho_\beta(x) \approx \frac{1+\pi^{-1}Q_\beta^2 x^2}{1+Q_\beta^2 x^2}, \quad (130)$$

where $\rho_\beta(x)$ interpolates the damping factor from $D_\beta(x) \approx 1$ for $Q_\beta x < 1$ to

$$D_\beta(x) \approx \sqrt{\frac{\pi}{2Q_\beta x}} \quad (131)$$

for $Q_\beta x \gg 1$.

For $Q_\beta x \gg 1$, the phase $\phi_\beta(x)$ saturates at $\pi/4$ compared to $\pi/2$ in the case of $\phi_{\rm sol}(x)$. For $Q_\beta x < 1$, the interpolation function $\rho_\beta(x) \approx 1$, while for $Q_\beta x \gg 1$, it only controls small details of saturation at $\pi/4$ so that the corresponding running spin tune can be approximated by

$$\nu_{\rm SF}^\beta(x) \approx \nu_{\rm SF}\left(1-\frac{Q_\beta}{1+4Q_\beta^2 x^2}\right). \quad (132)$$

Here, $\nu_{\rm SF}$ is the SF tune defined by Eqs. (31) and (33). In summary, despite the very different hierarchy of frequencies involved, the synchrotron and betatron oscillations have quite a similar impact on the SF dynamics.

VI. IMPACT OF THE FEEDBACK TO COMPENSATE FOR THE SPIN PRECESSION WALK DURING SPIN FLIP

So far, the spin phase walk has only been studied by the JEDI collaboration in the idle precession experiment (Fig. 1, [20]). In the regime of idle precessions, the spin phase walk measured in the time interval $t_{\rm fb}$ was compensated by varying the spin-precession frequency $f_{\rm s} = G\gamma f_{\rm rev}$ via a change of the beam revolution frequency $f_{\rm rev}$. In the regime of multiple spin flips, one has to invoke the pilot-bunch comagnetometry [29] and match the WF frequency $f_{\rm WF}$ to $f_{\rm s}$, correspondingly. In the actual experiment [20], the phase walk was measured about every second and the feedback was applied at somewhat irregular time intervals of the order of $t_{\rm fb} \approx 3$ s. In a simplified pattern, the phase walk $\sigma_{\rm fb}(n)$ in the first feedback interval $t_{\rm fb}$ is compensated by a judicious preemptive correction to $f_{\rm WF}$ in the next interval $t_{\rm fb}$, so that on average, the feedback corrected $\sigma_{\rm fb}(n) = \theta_{\rm s}(n) - \theta_{\rm WF}(n)$ averages to zero over one feedback period $t \in [0, 2t_{\rm fb}]$

$$\langle \sigma_{\rm fb}(n)\rangle = 0, \quad (133)$$

thereby producing a vanishing time-averaged detuning $\delta = 0$.

As such, $\sigma_{\rm fb}(n)$ is analogous to the SO-driven mismatch of spin precession and WF phases, apart from one distinction. Individual particles in the bunch have different SO amplitudes and correspondingly different time dependencies of the SF phases. In contrast to that, the spin-precession frequency walk, mediated by instabilities of the ring elements, is a collective effect, identical for all particles in the bunch. With a typical feedback interval time of $t_{\rm fb} \approx 3$ s, the feedback frequency $f_{\rm fb} \approx 0.17$ Hz is larger than the typical SF frequency $f_{\rm SF} = 0.08$ Hz in the pilot-bunch experiment [29]. In the important case of searching for a signal of the EDM of deuterons in the JEDI storage ring experiment, even smaller $f_{\rm SF}$ is of particular importance, see Ref. [37] and Sec. VIII.

Allowance for the feedback adds still another level in the hierarchy of frequencies. The action of a fast feedback on slow spin flips will be described by the spin envelope transfer matrix $\mathbf{U}_{\rm fb}(n)$, given in Eq. (110), subject to the substitution $C_{\rm WF}\Delta\theta_{\rm s}(n) \to \sigma_{\rm fb}$. In the application of the BK-averaging over the feedback phase, we make use of

$$\langle \sigma_{\rm fb}(n)\rangle = 0, \quad (134)$$

and obtain

$$\mathbf{U}_{\rm fb}(n) = \frac{1}{2}\chi_{\rm WF}\langle\cos\sigma_{\rm fb}(n)\rangle\mathbf{U}, \quad (135)$$

where $\mathbf{U}$ is given by Eq. (13). The net result amounts to a feedback-induced reduction of the SF tune:

$$\nu_{\rm SF}^{\rm (fb)} = \nu_{\rm SF}^0\langle\cos\sigma_{\rm fb}(n)\rangle. \quad (136)$$

Supposing a Gaussian distribution of the spin-phase walk, we obtain the reduction factor of the SF tune

$$C_{\rm fb} = \langle\cos\sigma_{\rm fb}(n)\rangle \approx \exp\left(-\frac{1}{2}\langle\sigma_{\rm fb}^2\rangle\right). \quad (137)$$

The above toy model estimate in Eq. (137) holds for $f_{\rm fb} \gg f_{\rm SF}$. We expect a similar spin-precession phase walk for the regimes of idle spin precession and continuous spin flips. Taking as a guidance, the experimental idle spin precession result $\sigma_{\rm fb} = \langle\sigma_{\rm fb}^2(n)\rangle^{1/2} = 0.2$ [18], we expect a

reduction of $C_{\rm fb}$ from 1 by a few %. One can test this conclusion by confronting the measured spin-flip frequency $f_{\rm SF}$ to an expectation from field maps of the spin flipper. Besides that, one can resort to numerical simulations based on the recorded feedback history.

VII. SPIN TOMOGRAPHY OF SYNCHROTRON OSCILLATIONS

The remarkable feature of the SF tune, given in Eq. (113), is its dependence on the SO amplitude, which can be tested experimentally tagging events in the polarimeter by their angular coordinate ϕ. The first look at this effect was undertaken in the pilot bunch experiment [29], where the full data sample of $\phi\in[-\xi_{\rm max},\xi_{\rm max}]\sigma_{\rm sy}=[-2,2]\sigma_{\rm sy}$ was split into the central set I (with $\phi\in[-\xi_{\rm med},\xi_{\rm med}]\sigma_{\rm sy}=[-0.6,0.6]\sigma_{\rm sy}$) and set II (with $\xi\in[\xi_{\rm med},\xi_{\rm max}]$), to be referred to as the head and tail set. The median $\xi_{\rm med}=0.6$ was chosen to have about the same number of recorded events in the sets I and II.

Particles in the bunch do perpetually oscillate from the head to tail and vice versa, crossing back and forth the central region $\xi\le\xi_{\rm med}|$, and a fraction of the time they spend at $|\phi_{\rm med}|<|\phi|<|\phi_{\rm max}|$ is given by the duty cycle

$$\mathcal{D}(\xi_{\rm max},\xi_{\rm med},\xi^2)=\frac{2}{\pi}\left[\arccos\left(\frac{\xi_{\rm med}}{\xi}\right)-\arccos\left(\frac{\xi_{\rm max}}{\xi}\right)\right]. \tag{138}$$

For arbitrary domain $\mathcal{R}$, the expectation value of the phase factor is given by

$$\langle\exp(ix(\xi))\rangle_\xi=\frac{\int_{\mathcal{R}}d\xi F(\xi)\mathcal{D}(\mathcal{R},\xi^2)\exp(ix(\xi))}{\int_{\mathcal{R}}d\xi F(\xi)\mathcal{D}(\mathcal{R},\xi^2)}. \tag{139}$$

The integrand in Eq. (139) has remarkable factorization properties. Consider the set $\mathcal{R}$ of $\xi\ge\xi_{\rm m}$. In terms of the convenient new variable $\zeta_{\rm sy}=\xi^2-\xi_{\rm m}^2$, the expansion of Eq. (115) gives $J_0(\xi C_{\rm WF}\psi_{\rm sy})\approx J_0(\xi_{\rm m}C_{\rm WF}\psi_{\rm sy})-Q_{\rm sy}\zeta_{\rm sy}$ so that the phase factor in the integrand factorizes. A similar factorization works for the Gaussian factor in $F(\xi)$, and we obtain

$$\begin{aligned}&\langle\exp(ix(\xi))\rangle_\xi\\&=\exp(ix(\xi_{\rm m}))\\&\quad\times\frac{\int_{\mathcal{R}}d\zeta\mathcal{D}(\mathcal{R},\xi_{\rm m}^2+\zeta_{\rm sy})\exp(-(1+iQ_{\rm sy}x)\zeta_{\rm sy})}{\int_{\mathcal{R}}d\zeta\mathcal{D}(\mathcal{R},\xi_{\rm m}^2+\zeta_{\rm sy})\exp(-\zeta_{\rm sy})}.\end{aligned} \tag{140}$$

In the generic case, the duty cycle prevents an analytic integration. For the sake of illustration, consider the domain $\mathcal{R}=[\infty,\xi_{\rm m}]$. For sufficiently large $\xi_{\rm m}>1$, one can use the approximation $\mathcal{D}(\infty,\xi_{\rm m},\xi^2)\approx\sqrt{\zeta_{\rm sy}/\xi_{\rm m}^2}$. Then the integrals in Eq. (140) reduce to the Euler gamma functions with the result:

$$\langle\exp(ix(\xi))\rangle_\xi\approx\frac{\exp(ix(\xi_{\rm m}))}{1+iQ_{\rm sy}(\xi_{\rm m})x}, \tag{141}$$

where $Q_{\rm sy}(\xi_{\rm m})=C(\xi_{\rm m})Q_{\rm sy}(\xi_{\rm m})$, and $C(\xi_m\gg1)=3/2$, while for $\xi_{\rm m}=0$, Eq. (120) corresponds to $C(0)=1$. Hence, we predict a more rapid depolarization of the head and tale portions of the bunch:

$$\frac{S_{\rm s}(\infty,\xi_{\rm m})}{S_{\rm s}(\infty,0)}\sim\sqrt{\frac{1+Q_{\rm sy}^2x^2}{1+C^2(\xi_{\rm m})Q_{\rm sy}^2x^2}}. \tag{142}$$

As another case of spin-flip tomography, we comment on the thought experiment with incomplete masking (gating-out) of the pilot bunch, in which the head and tail particles of the pilot bunch are subjected to spin-flips by the rf field of the WF, while the central body of the bunch is shielded from the rf field of the WF. The interplay between the finite time duration of the gate and the bunch length is as follows. At each turn, the head of the bunch with $\phi>\xi_{\rm m}\sigma$ crosses the WF still in operation, and the spins in the bunch are subjected to the spin-flip kicks. The main part of the bunch traverses the already switched-off WF. In terms of SF, this masking can be considered as an operation of the WF with $\chi_{\rm WF}=0$. Since these particles spend part of the time in the central region of the bunch, their depolarization will mimic a partial depolarization of the central part of the bunch.

Equally important would be an analysis of the experimental data on the revolution-phase tagged oscillation amplitude, which would amount to a spin tomography of the longitudinal polarization profile in a static bunch. As emphasized in Sec. I, the knowledge about the nonuniformity of the longitudinal polarization profile of colliding bunches is relevant for a quantitative interpretation of double polarization observables in collider experiments (see Ref. [39] for a related discussion of the impact of transverse bunch polarization profile observed at RHIC [38]).

The above discussion can also be extended to transverse spin tomography of beam bunches. The transverse profile of the polarization was previously studied at RHIC, where a significant variation of the transverse polarization from the core to the skin particles in the beam was observed [38]. In this case, the skin is populated by particles having large betatron amplitudes, while alongside the particles with small betatron amplitudes also large-amplitude particles spend part of their time in the core region.

VIII. IMPLICATIONS FOR SPIN-FLIP TUNE MAPPING

Here, we explore implications of detuning and spin decoherence on the search for the EDM of charged particles in all magnetic storage rings with emphasis on the activity of the JEDI collaboration.

The signal for an EDM is the spin precession of particles spin in an electric field. In the comoving frame in a magnetic field, the spins of charged particles are subjected to the electric field generated by the Lorentz transformation. The familiar Frenkel-Thomas-BMT result for the angular velocity of the idle spin precession with respect to the particle momentum in a homogeneous magnetic field reads [22,23,51–54]:

$$\vec{\Omega} = -\frac{q}{m}\left[G\vec{B} + \left(\frac{1}{\beta^2} - 1 - G\right)\vec{\beta}\times\vec{E} + \frac{1}{2}\eta_{\mathrm{EDM}}(\vec{E} + [\vec{\beta}\times\vec{B}])\right], \tag{143}$$

where η_{EDM} defines the EDM in units of the nuclear magneton via $d = \eta_{\mathrm{EDM}} q/(2m)$.

Of major concern in this section will be the imperfection magnetic fields and we invoke the momentum frame $\{\vec{e}_x, \vec{e}_y, \vec{e}_z\}$ of Fig. 1. In an ideal purely magnetic ring, $\vec{B}$ is normal to the ring plane and the EDM tilts the spin stable axis $\vec{e}_{\mathrm{s}}$ according to

$$\xi^{\mathrm{EDM}} = \arctan\left(\frac{\eta_{\mathrm{EDM}}}{2G\beta}\right),$$
$$\vec{e}_{\mathrm{s}} = \sin\xi^{\mathrm{EDM}}\vec{e}_{\mathrm{r}} + \cos\xi^{\mathrm{EDM}}\vec{e}_y. \tag{144}$$

If the WF axis was aligned perpendicular to the momentum plane [55], $\vec{w} = \vec{e}_y$, Eq. (19) would yield

$$|\vec{e}_{\mathrm{s}}\times\vec{w}| = \sin\xi^{\mathrm{EDM}} \quad \text{and} \quad \nu_{\mathrm{SF}} = \frac{1}{4\pi}\nu_{\mathrm{WF}}\sin\xi^{\mathrm{EDM}}, \tag{145}$$

and the experimental measurement of the SF tune ν_{SF} would amount to the measurement of the EDM of the particle [9,56]. However, imperfection magnetic fields are endemic in realistic all-magnetic rings like COSY and tilt the spin stable axis which acquires tangential a_z^{MDM} and radial a_x^{MDM} components so that

$$\vec{e}_{\mathrm{s}} \Rightarrow \vec{e}_y + \sin\xi^{\mathrm{EDM}}\vec{e}_x + a_x^{\mathrm{MDM}}\vec{e}_{\mathrm{r}} + a_z^{\mathrm{MDM}}\vec{e}_z. \tag{146}$$

The interaction of the magnetic dipole moment (MDM) of the stored particles with imperfection fields may overwhelm the EDM effect in the SF tune ν_{SF} [9].

Nevertheless, one can resort to an active compensation of the intrinsic imperfections by two artificial imperfections (AI). Specifically, what matters for the SF rate is contained in the cross product $|\vec{e}_{\mathrm{s}}\times\vec{w}|$. For the first time, this approach with two cooler solenoids in two straight sections acting as two AIs was experimentally studied at COSY [9] (see also [37]). When transferred to the spin flipper location, the local longitudinal AI fields acquire radial components as well. In the recent experiment with stored deuterons in the COSY ring, one of the solenoids was substituted by rotating the transverse magnetic field axis of the rf WF around the longitudinal axis [57]. The stable spin axis $\vec{e}_{\mathrm{s}}$ in the ring is tilted by the static magnetic field of the Siberian snake in the straight section opposite the WF, which rotates the spins around the z axis by an angle χ^{sol}, while the magnetic field axis $\vec{w}$ of the WF is tilted by a rotation of WF itself around the z axis by an angle ϕ^{WF}. Since the solenoid fields affect the spin precession tune [9], the WF frequency has to be corrected accordingly.

For small WF rotation angles, we have $\vec{w} \approx \vec{e}_x + \phi^{\mathrm{WF}}\vec{e}_y$ and, in the case of the exact resonance, one finds

$$\nu_{\mathrm{SF}} = \frac{C_{\mathrm{fb}}\chi_{\mathrm{WF}}}{4\pi}|\vec{e}_{\mathrm{s}}\times\vec{w}| = \frac{\chi_{\mathrm{WF}}}{4\pi}\left[(\xi^{\mathrm{MDM}} + a_x^{\mathrm{MDM}} - \phi^{\mathrm{WF}})^2 + \left(a_z^{\mathrm{MDM}} + \frac{1}{2\sin\pi\nu_{\mathrm{s}}}\chi^{\mathrm{sol}}\right)^2\right]^{1/2}. \tag{147}$$

The search for the deuteron EDM was carried out with spin phase feedback switched on, and in the above equation, the feedback correction factor C_{fb} is included. As a function of the artificial imperfection parameters, ϕ^{WF} and χ^{sol}, the SF tune ν_{SF} describes an elliptic cone. The corresponding numerical simulations of the strosocopic spin evolution were reported in Fig. 20(a) of [37]. The accuracy with which the location of the vertex of the cone at $\nu_{\mathrm{SF}} = 0$ can be determined defines the best accuracy with which ξ_{EDM} can be determined using the described technique [57]. Barring accidental cancellations, one can reinterpret this accuracy as a tentative upper bound for ξ^{EDM}.

At finite detuning, the observed SF tune will be modified according to Eq. (33), yielding

$$\nu_{\mathrm{SF}} = \frac{C_{\mathrm{fb}}}{4\pi}\left\{\chi_{\mathrm{WF}}^2\left[(\xi^{\mathrm{MDM}} + a_x^{\mathrm{MDM}} - \phi^{\mathrm{WF}})^2 + \left(a_z^{\mathrm{MDM}} + \frac{1}{2\sin\pi\nu_{\mathrm{s}}}\chi^{\mathrm{sol}}\right)^2\right] + \frac{1}{4}\delta^2\right\}^{1/2}. \tag{148}$$

The feedback is expected to produce a vanishing permanent detuning such that $\delta = 0$. Varying the feedback factor C_{fb} from fill to fill would not affect the location of the vertex of the cone, but would degrade the fit quality with respect to the χ^2 if C_{fb} were constant and equal to unity.

In the absence of comagnetometry, one could try to extract the SF tune $\nu_{\rm SF}$ from the time dependence of the SF phase in the small-x corner of the first quadrant:

$$\left.\frac{\mathrm{d}p_{\rm s}(x)}{\mathrm{d}t}\right|_{\rm t=0} = -\sin\Phi_{\rm in}\frac{\mathrm{d}x}{\mathrm{d}t} = -2\pi f_{\rm rev}\sin\Phi_{\rm in}\nu_{\rm SF}. \tag{149}$$

To go beyond the first quarter of the spin-flip period and exploit the full statistical accuracy of the cycle, one needs to invoke pilot-bunch comagnetometry [29].

Once the SOs come into play, the nonlinear phase walk $\varphi_{\rm sy}(x)$, which drives the spin-flip due to spin decoherence, must be considered [see Eq. (125)]. As far as the JEDI experimental data were taken in the regime of $Q_{\rm sy}x < 1$, as suggested by the above cited evaluations of $Q_{\rm sy}$ from Eq. (116), the major effect will be a minor correction to the visible spin-flip tune:

$$\nu_{\rm SF}^{\rm (exp)} \approx (1 - Q_{\rm sy})\nu_{\rm SF}, \tag{150}$$

which is extra to the feedback-driven renormalization in Eq. (148). However, where $Q_{\rm sy}x \sim 1$, then it would have been necessary to directly use the nonlinear $\varphi_{\rm sy}(x)$ in the extraction of $\nu_{\rm SF}$ from the experimental spin-flip data. The same point refers to the spin decoherence controlled by betatron oscillations.

IX. SUMMARY AND CONCLUSIONS

Inspired by the JEDI studies of high-precision spin dynamics aiming at the search for the EDM of charged particles using storage rings and the recently developed pilot-bunch approach to comagnetometry and manipulation of polarization of selected bunches in storage rings, we have developed a theoretical description of rf-driven spin rotations that account for spin decoherence effects and detuning away from the exact spin resonance. The fully analytical description of the multiple spin flips, comprising the polarimetry of in-plane polarization components and various spin decoherence mechanisms, is essential for the data analysis of the EDM experiments carried out at COSY. The experiments exhibit a level of precision that requires a thorough understanding of the polarization evolution in the ring in the presence of an rf WF, a solenoid magnet, and non-negligible ring imperfections.

In the framework of Bogoliubov-Krylov approach to rf-driven spin rotations, based on the frequency hierarchy in the problem, we have presented results for the Bloch phenomenology of depolarization and more dynamical models of spin decoherence, mediated by synchrotron oscillations and noncompensated orbit lengthening by betatron oscillations. We found substantial similarities between synchrotron oscillations and betatron oscillations as driving sources of spin decoherence, with nonexponential depolarization to rf-driven spin rotations detuned spin precession being a common denominator. Interestingly, in the presence of ring instabilities, the feedback mechanism invoked to maintain the most accurate phase locking between the rf WF and the spin precession is shown to reduce the spin-flip frequency. This effect is of importance for the interpretation of searches for the EDM of charged particles in storage rings.

It has been shown that different spin-decoherence models result in different patterns of depolarization of different components of the continuously flipping polarization. We emphasized the importance of a concurrent analysis of vertical and in-plane precessing polarization components, in particular, the previously unexplored phase of the in-plane polarization envelope, as an additional insight into the dynamics of rf-driven spin oscillations in storage rings.

The synchrotron oscillation mechanism of decoherence is shown to be governed by the bunch length, which is a function of the SO amplitude, and we suggest a spin-flip-based tomography of the SO-driven spin dynamics. The latter provides access to the hitherto unexplored longitudinal profile of the beam polarization in a bunch, which is important to quantify the polarization-dependent luminosity in collider experiments. Within the statistical accuracy currently achieved, the main results of the pilot bunch experiment are consistent with the quantitative expectations of the synchrotron oscillation model.

ACKNOWLEDGMENTS

The work presented here has been performed in the framework of the JEDI collaboration and was supported by an ERC Advanced Grant of the European Union (Proposal No. 694340: Search for electric dipole moments using storage rings) and by the Shota Rustaveli National Science Foundation of the Republic of Georgia (SRNSFG Grant No. DI-18-298: High-precision polarimetry for charged particle EDM searches in storage rings). This research is part of a project that has received funding from the European Union's Horizon 2020 research and innovation program under Grants Agreement No. STRONG-2020 and No. 824093. The work of A. A., A. M., and N. N. N. on the topic was supported by the Russian Science Foundation (Grant No. 22-42-04419). Thanks are due to A. Zelenski for useful discussions.

[1] F. Rathmann, B. von Przewoski, W. A. Dezarn, J. Doskow, M. Dzemidzic, W. Haeberli, J. G. Hardie, B. Lorentz, H. O. Meyer, P. V. Pancella, R. E. Pollock, T. Rinckel, F. Sperisen, and T. Wise, Complete angular distribution measurements of pp spin correlation parameters A_{xx}, A_{yy}, and A_{xz} and analyzing power A_y at 197.4 MeV, Phys. Rev. C **58**, 658 (1998).

[2] S. Y. Lee, *Spin Dynamics and Snakes in Synchrotrons* (World Scientific, Singapore, 1997).

[3] S. R. Mane, Y. M. Shatunov, and K. Yokoya, Spin-polarized charged particle beams in high-energy accelerators, Rep. Prog. Phys. **68**, 1997 (2005).

[4] F. Bloch, Nuclear induction, Phys. Rev. **70**, 460 (1946).

[5] I. I. Rabi, N. F. Ramsey, and J. Schwinger, Use of rotating coordinates in magnetic resonance problems, Rev. Mod. Phys. **26**, 167 (1954).

[6] A. Abragam, *The Principles of Nuclear Magnetism* (Oxford University Press, London, 1961).

[7] A. Abragam and M. Goldman, Principles of dynamic nuclear polarization, Rep. Prog. Phys. **41**, 395 (1978).

[8] In accelerator physics, f_s usually defines the spin rotation with respect to the particle momentum, i.e., f_s denotes the spin precession frequency in the laboratory frame with the beam revolution frequency subtracted.

[9] A. Saleev *et al.* (JEDI Collaboration), Spin tune mapping as a novel tool to probe the spin dynamics in storage rings, Phys. Rev. Accel. Beams **20**, 072801 (2017).

[10] I. Koop and Y. Shatunov, The spin precession tune spread in the storage ring, in *Proceedings of the 1st European Particle Accelerator Conference, EPAC-1988, Rome, Italy*, edited by S. Tazzari (World Scientific, Singapore, 1988), Vol. 1, 2, pp. 738–739.

[11] G. Guidoboni *et al.* (JEDI Collaboration), How to reach a thousand-second in-plane polarization lifetime with 0.97 GeV/c deuterons in a storage ring, Phys. Rev. Lett. **117**, 054801 (2016).

[12] G. Guidoboni *et al.* (JEDI Collaboration), Connection between zero chromaticity and long in-plane polarization lifetime in a magnetic storage ring, Phys. Rev. Accel. Beams **21**, 024201 (2018).

[13] A. N. Skrinsky and Y. M. Shatunov, Precision measurements of masses of elementary particles using storage rings with polarized beams, Sov. Phys. Usp. **32**, 548 (1989).

[14] M. Froissart and R. Stora, Depolarisation d'un faisceau de protons polarises dans un synchrotron, Nucl. Instrum. Methods **7**, 297 (1960).

[15] JEDI collaboration, http://collaborations.fz-juelich.de/ikp/jedi/.

[16] R. Maier, Cooler synchrotron COSY—Performance and perspectives, Nucl. Instrum. Methods Phys. Res., Sect. A **390**, 1 (1997).

[17] C. Weidemann *et al.*, Toward polarized antiprotons: Machine development for spin-filtering experiments, Phys. Rev. ST Accel. Beams **18**, 020101 (2015).

[18] D. Eversmann *et al.* (JEDI Collaboration), New method for a continuous determination of the spin tune in storage rings and implications for precision experiments, Phys. Rev. Lett. **115**, 094801 (2015).

[19] Z. Bagdasarian *et al.*, Measuring the polarization of a rapidly precessing deuteron beam, Phys. Rev. ST Accel. Beams **17**, 052803 (2014).

[20] N. Hempelmann *et al.* (JEDI Collaboration), Phase locking the spin precession in a storage ring, Phys. Rev. Lett. **119**, 014801 (2017).

[21] J. Slim *et al.* (JEDI Collaboration), First detection of collective oscillations of a stored deuteron beam with an amplitude close to the quantum limit, Phys. Rev. Accel. Beams **24**, 124601 (2021).

[22] V. Bargmann, L. Michel, and V. L. Telegdi, Precession of the polarization of particles moving in a homogeneous electromagnetic field, Phys. Rev. Lett. **2**, 435 (1959).

[23] T. Fukuyama and A. J. Silenko, Derivation of generalized Thomas-Bargmann-Michel-Telegdi equation for a particle with electric dipole moment, Int. J. Mod. Phys. A **28**, 1350147 (2013).

[24] F. Abusaif *et al.* (CPEDM Collaboration), Storage ring to search for electric dipole moments of charged particles: Feasibility study, CERN, Geneva, CERN Yellow Reports: Monographs, Report No. 2021-003, 2021, 10.23731/CYRM-2021-003.

[25] N. Hempelmann *et al.* (JEDI Collaboration), Phase measurement for driven spin oscillations in a storage ring, Phys. Rev. Accel. Beams **21**, 042002 (2018).

[26] V. Anastassopoulos *et al.*, A storage ring experiment to detect a proton electric dipole moment, Rev. Sci. Instrum. **87**, 115116 (2016).

[27] Z. Omarov, H. Davoudiasl, S. Haciomeroglu, V. Lebedev, W. M. Morse, Y. K. Semertzidis, A. J. Silenko, E. J. Stephenson, and R. Suleiman, Comprehensive symmetric-hybrid ring design for a proton EDM experiment at below 10^{-29} e · cm, Phys. Rev. D **105**, 032001 (2022).

[28] R. Alarcon *et al.*, Electric dipole moments and the search for new physics, arXiv:2203.08103.

[29] J. Slim *et al.*, Pilot bunch and co-magnetometry of polarized particles stored in a ring, arXiv:2309.06561.

[30] J. Slim, A. Nass, F. Rathmann, H. Soltner, G. Tagliente, and D. Heberling, The driving circuit of the waveguide RF Wien filter for the deuteron EDM precursor experiment at COSY, J. Instrum. **15**, P03021 (2003).

[31] J. Slim, F. Rathmann, A. Nass, H. Soltner, R. Gebel, J. Pretz, and D. Heberling, Polynomial Chaos Expansion method as a tool to evaluate and quantify field homogeneities of a novel waveguide RF Wien filter, Nucl. Instrum. Methods Phys. Res., Sect. A **859**, 52 (2017).

[32] J. Slim, R. Gebel, D. Heberling, F. Hinder, D. Hölscher, A. Lehrach, B. Lorentz, S. Mey, A. Nass, F. Rathmann, L. Reifferscheidt, H. Soltner, H. Straatmann, F. Trinkel, and J. Wolters, Electromagnetic simulation and design of a novel waveguide RF Wien filter for electric dipole moment measurements of protons and deuterons, Nucl. Instrum. Methods Phys. Res., Sect. A **828**, 116 (2016).

[33] I. A. Koop, Spin wheel approach, in *Proceedings of the 4th International Particle Accelerator Conference, IPAC 2013, Shanghai, China*, edited by Z. Dai, C. Petit-Jean-Genaz, V. R. W. Schaa, and C. Zhang (JACoW, Geneva, Switzerland, 2013), TUPWO040.

[34] P. Benati *et al.*, Synchrotron oscillation eqects on an rf-solenoid spin resonance, Phys. Rev. ST Accel. Beams **15**, 124202 (2012).

[35] N. N. Bogoliubov and Y. A. Mitropolsky, Asymptotic methods in the theory of non-linear oscillations, *International Monographs on Advanced Mathematics and Physics* (Gordon and Breach, New York, 1961).

[36] A. J. Silenko, General classical and quantum-mechanical description of magnetic resonance: An application to electric-dipole-moment experiments, Eur. Phys. J. C **77**, 341 (2017).

[37] F. Rathmann, N. N. Nikolaev, and J. Slim, Spin dynamics investigations for the electric dipole moment experiment, Phys. Rev. Accel. Beams **23**, 024601 (2020).

[38] I. Nakagawa, I. Alekseev, A. Bazilevsky, A. Bravar, G. Bunce, S. Dhawan, K. O. Eyser, R. Gill, W. Haeberli, H. Huang, Y. Makdisi, A. Nass, H. Okada, E. Stephenson, D. N. Svirida, T. Wise, J. Wood, K. Yip, and A. Zelenski, RHIC polarimetry, Eur. Phys. J. Special Topics **162**, 259 (2008).

[39] W. Fischer and A. Bazilevsky, Impact of three-dimensional polarization profiles on spin-dependent measurements in colliding beam experiments, Phys. Rev. ST Accel. Beams **15**, 041001 (2012).

[40] Ya. S. Derbenev, A. M. Kondratenko, and A. N. Skrinskii, Dynamics of the polarization of particles near spin resonances, J. Exp. Theor. Phys. **33**, 658 (1971), http://www.jetp.ras.ru/cgi-bin/e/index/e/33/4/p658?a=list.

[41] E. Kovács, Rotation about an arbitrary axis and reflection through an arbitrary plane, Annales Mathematicae et Informaticae **40**, 175 (2012), https://ami.uni-eszterhazy.hu/uploads/papers/finalpdf/AMI_40_from175to186.pdf.

[42] V. S. Morozov, Z. B. Etienne, M. C. Kandes, A. D. Krisch, M. A. Leonova, D. W. Sivers, V. K. Wong, K. Yonehara, V. A. Anferov, H. O. Meyer, P. Schwandt, E. J. Stephenson, and B. von Przewoski, First spin flipping of a stored spin-1 polarized beam, Phys. Rev. Lett. **91**, 214801 (2003).

[43] S. Karanth *et al.* (JEDI Collaboration), First search for axionlike particles in a storage ring using a polarized deuteron beam, Phys. Rev. X **13**, 031004 (2023).

[44] Recall the classic example of the frequency shift of the damped harmonic oscillator: $z(t) = A\exp(-\gamma t) \times \sin(\sqrt{\omega_0^2 - \gamma^2}t + \phi_0)$.

[45] A. Saleev, N. N. Nikolaev, F. Rathmann, F. Hinder, J. Pretz, and M. Rosenthal, Non-exponential decoherence of radio-frequency resonance rotation of spin in storage rings, Pis'ma Zh. Eksp. Teor. Fiz. **106**, 199 (2017) [JETP Lett. **106**, 213 (2017)].

[46] Note that the Abel integral representation in Eq. (96) is entirely different from the standard representation of the Rayleigh distribution as a derivative of the Gaussian cumulative distribution.

[47] S.-Y. Lee, *Accelerator Physics*, 4th ed. (World Scientific Publishing Company, Singapore, 2018).

[48] A. Lehrach, B. Lorentz, W. Morse, N. Nikolaev, and F. Rathmann, Precursor experiments to search for permanent electric dipole moments (EDMs) of protons and deuterons at COSY, arXiv:1201.5773.

[49] A treatment of the side band resonances at $f_{\rm WF} = f_{\rm s} + Kf_{\rm sy}$ (with $K = \pm 1, \pm 2, \ldots$) [40] is beyond the scope of this paper.

[50] A discussion of the impact of Siberian snakes on the continuous spin flips is beyond the scope of the present study.

[51] J. Frenkel, Spinning electrons, Nature (London) **117**, 653 (1926).

[52] J. Frenkel, Die Elektrodynamik des rotierenden Elektrons, Z. Physik **37**, 243 (1926).

[53] L. H. Thomas, The motion of the spinning electron, Nature (London) **117**, 514 (1926).

[54] L. H. Thomas, The kinematics of an electron with an axis, Phil. Mag. Ser. 7 **3**, 1 (1927).

[55] We refer to this orientation as the EDM mode.

[56] G. W. Bennett *et al.* (Muon (g-2) Collaboration), Improved limit on the muon electric dipole moment, Phys. Rev. D **80**, 052008 (2009).

[57] The JEDI collaboration has successfully conducted two experimental campaigns with the aim to perform the first direct measurement of the deuteron EDM at COSY. The data analysis is in progress. Presently, the collaboration is performing a number of additional systematic investigations. A corresponding publication on the deuteron EDM experiment is in preparation.